

# **Tectonics**°

# **RESEARCH ARTICLE**

10.1029/2024TC008371

### **Special Collection:**

Alpine mountain belts in 4-dimensions

### **Key Points:**

- Exhumation of the western Tauern
  Window occurred in two phases—first
  viscous folding and second displacement along the Sub-Tauern ramp
- Viscous folding started to cease slightly earlier than 17 ± 0.6 Ma, when a geothermal gradient of 50°C/km prevailed
- The Subpenninic core was not affected by W-E extension, while the hangingwall nappes experienced thinning of 25%-48%

### **Supporting Information:**

Supporting Information may be found in the online version of this article.

### Correspondence to:

### J. Rudmann,

Julia.Rudmann@liag-institut.de; julia.rudmann@gmx.de

### Citation:

Rudmann, J., Tanner, D. C., Stipp, M., Pomella, H., & Brandes, C. (2025). 2-D kinematic restoration of the western Tauern Window, eastern Alps using thermochronological and P-T constraints. *Tectonics*, 44, e2024TC008371. https://doi.org/10.1029/2024TC008371

Received 11 APR 2024 Accepted 13 JUN 2025

### **Author Contributions:**

Funding acquisition: D. C. Tanner, M. Stipp, C. Brandes Investigation: J. Rudmann Methodology: J. Rudmann, D. C. Tanner, M. Stipp, H. Pomella, C. Brandes Supervision: D. C. Tanner, M. Stipp, H. Pomella

Visualization: J. Rudmann, H. Pomella Writing – original draft: J. Rudmann, H. Pomella, C. Brandes

© 2025. The Author(s).

This is an open access article under the terms of the Creative Commons

Attribution License, which permits use, distribution and reproduction in any medium, provided the original work is properly cited.

# 2-D Kinematic Restoration of the Western Tauern Window, Eastern Alps Using Thermochronological and P-T Constraints

J. Rudmann<sup>1,2</sup> , D. C. Tanner<sup>1</sup> , M. Stipp<sup>2</sup> , H. Pomella<sup>3</sup> , and C. Brandes<sup>4</sup>

<sup>1</sup>LIAG Institute for Applied Geophysics, Hannover, Germany, <sup>2</sup>Martin Luther University Halle-Wittenberg, Halle/Saale, Germany, <sup>3</sup>University of Innsbruck, Innsbruck, Austria, <sup>4</sup>Leibniz University Hannover, Hannover, Germany

**Abstract** The Penninic and Subpenninic nappe stack of the Tauern Window (TW) in the European Alps was formed by collision between Europe (Subpenninic) and the Adria margin (Austroalpine), and finally exhumed by the northward push of the Southalpine Dolomites indenter in the Miocene. In this study, we kinematically restore a cross-section along the trace of the Brenner Base Tunnel, concentrating mainly on the Subpenninic nappes (Venediger duplex; VD). We integrate zircon fission-track data (ZFT) as a temporal constraint for the termination of viscous deformation and test different geothermal gradients (GG). P-T-t data are used to define (a) the depth of the brittle-viscous transition (ca.  $300^{\circ}$ C) and (b) pre-indenter depth. We displace the VD down along the Sub-Tauern ramp below the  $300^{\circ}$ C isotherm. At that time, a GG of ca.  $50^{\circ}$ C/km prevailed. ZFT data reveal that viscous conditions allowing folding of the VD started to cease slightly earlier than  $17 \pm 0.6$  Ma. Unfolding of the VD, while conserving surface area, yield that the model is extended by ca. 70 km (thus equaling indenter shortening), which means that in the westernmost TW, the VD was not significantly affected by W-E extension. Reconstruction of the hanging-wall nappes (Austroalpine and Penninic nappes) above the restored VD reveals that the total pre-indenter thickness of their northern limbs was 25%—48% greater than today. We interpret this as tectonic thinning, which was mainly caused by the Brenner normal fault.

# 1. Introduction

The Tauern Window (TW) and its adjacent areas within the European Eastern Alps (Figure 1a) underwent a polyphase tectonic history. In addition to the Variscan deformation of the basement units, the area experienced two distinct Alpine orogenic phases: (a) The Cretaceous Eoalpine event, which was caused by a westward-directed movement of Austroalpine nappes (Adria-derived), and (b) the Cenozoic Neoalpine orogeny, characterized by nearly northward convergence (e.g., Foitzheim et al., 1994; Handy et al., 2010; Neubauer, 1994; Schmid et al., 2004). The latter started with the subduction of the Penninic Ocean in southerly direction underneath the Adriatic plate (e.g., Frisch, 1979; Froitzheim et al., 1994; Handy et al., 2010; Schmid et al., 2004, 2013). Convergence resulted in the closure of the Penninic Ocean and the subduction and accretion of the southern margin of Europe (Subpenninic). Subsequently, in the Late Eocene and Early Oligocene, duplexing of the lower plate (Subpenninic) and nappe-stacking within the orogenic wedge was initiated (Schmid et al., 2013). At that time, the W-E-striking Periadriatic fault system, one of the major fault systems in the European Alps, was activated as a dextral fault system, separating the Western, Central and Eastern Alps from the Southern Alps. Intrusions were emplaced along the Periadriatic fault system (e.g., Berger et al., 2024; Rosenberg, 2004; von Blanckenburg & Davies, 1995), which were subsequently synkinematically sheared and rotated (e.g., Pomella et al., 2011; Stipp et al., 2004).

The final deformation phase (according to Schmid et al., 2013) was initiated by the northward push of the Dolomites indenter (eastern Southern Alps). In the Late Oligocene, the previously straight, W-E-striking Periadriatic fault system was first bent (represented by the Meran Mauls fault; Pomella et al., 2011, 2012) and, subsequently, sinistrally offset along the Giudicarie fault system in the Late Oligocene/Early Miocene (e.g., Neubauer et al., 2000; Pomella et al., 2011, 2012; Ratschbacher, Frisch, et al., 1991; Scharf et al., 2013). This offset accounts ca. 75 km at present, including the offset along the Giudicarie fault system and the Meran Mauls fault (e.g., Favaro et al., 2017 and references therein; Verwater et al., 2021). This corresponds to a ca. 70 km northward motion of the Dolomites indenter (Figure 1a). In front of the Dolomites indenter, the Miocene shortening led to (a) upright folding of the Subpenninic core of the western TW (e.g., Lammerer & Weger, 1998; Lammerer et al., 2008; Rosenberg et al., 2018 and references therein, Schmid et al., 2013 and references therein) and to (b) orogen-

RUDMANN ET AL. 1 of 22

from https://agupubs.onlinelibrary.wiley.com/doi/10.1029/2024TC008371 by Martin Luther University Halle-Wittenberg, Wiley Online Library on [16/10/2025]. See the Terms and Conditions

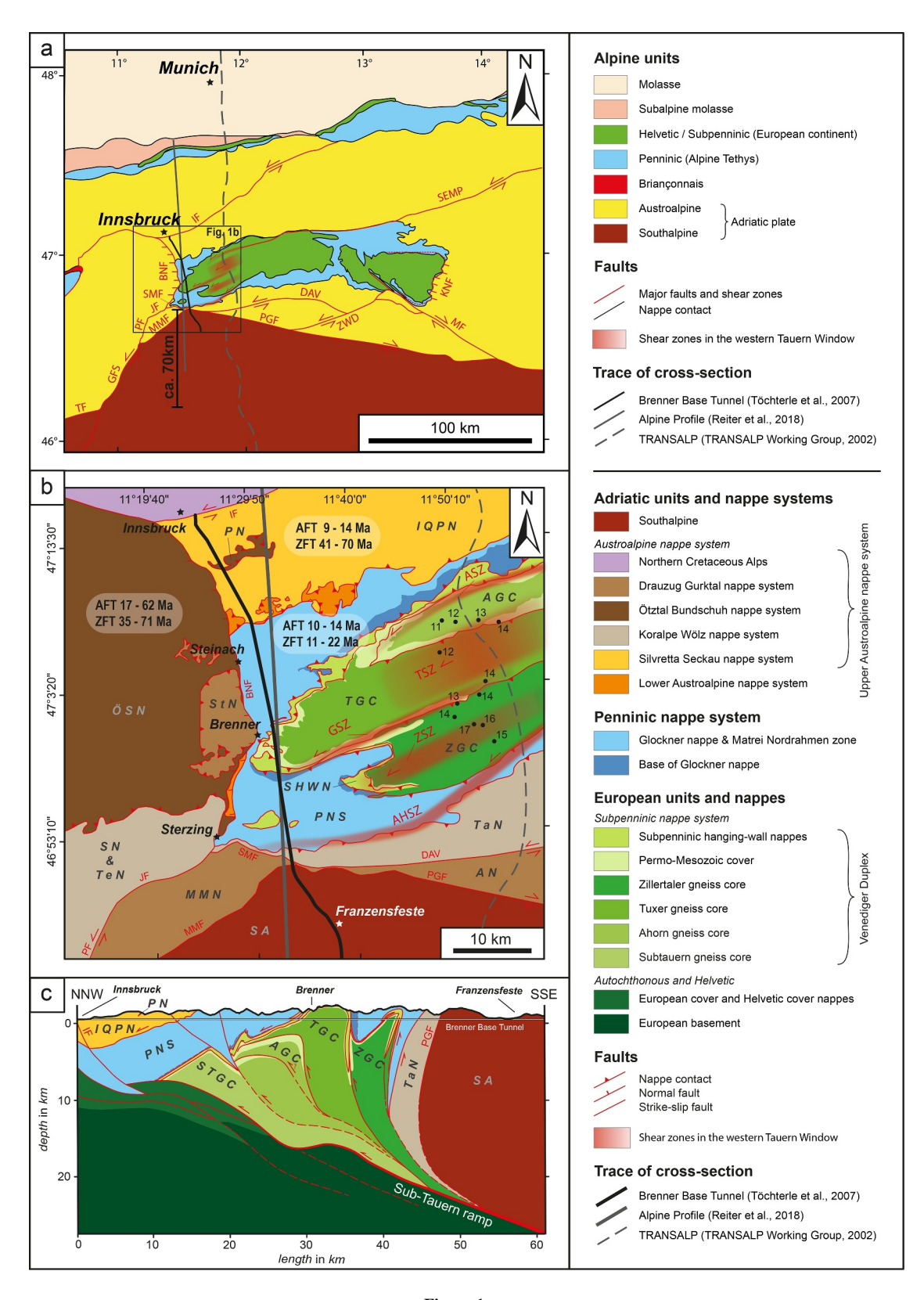


Figure 1.

RUDMANN ET AL. 2 of 22

parallel extension. The latter is expressed by normal faults, bounding the TW to the east (Katschberg normal fault, KNF; e.g., Genser & Neubauer, 1989) and west (Brenner normal fault, BNF; e.g., Behrmann, 1988; Selverstone, 1988), and by lateral extrusion toward the east, along major strike-slip faults, such as the Inntal fault, the Salzach Ennstal Mariazell-Puchberg fault (SEMP), the Mölltal fault and the Pustertal Gailtal fault (Figures 1a and 1b; e.g., Frisch et al., 2000; Linzer et al., 2002; Ratschbacher, Frisch, et al., 1991; Ratschbacher, Merle, et al., 1991; Rosenberg et al., 2018). All these processes, in combination with erosion, are assumed to have acted contemporaneously (e.g., Favaro et al., 2017; Ratschbacher, Frisch, et al., 1991; Ratschbacher, Merle, et al., 1991; Ricchi et al., 2020; Scharf et al., 2013; Schmid et al., 2013 and references therein) and led to vertical exhumation of the western TW by 23–25 km (Fügenschuh et al., 1997; von Blanckenburg et al., 1989).

**Tectonics** 

As this summary above shows, much research has already been done on the TW. Nevertheless, the precise deformation processes (i.e., the amount and timing of viscous folding compared to the amount of slip along the Sub-Tauern ramp) that occurred within the Tauern region remain insufficiently understood. Our study aims to understand the tectonic processes involved in the formation and exhumation of the western TW, and therefore to quantify the deformation undergone by the nappe systems of the western TW during the indenter stage as much as possible, and present one possible pre-indenter structure (which is not known as yet). For this purpose, we restore a cross-section along the trace of the Brenner Base Tunnel to the point in time before indentation began. We choose the cross-section along the Brenner Base Tunnel, because it runs approximately parallel to the tectonic transport direction (e.g., Eizenhöfer et al., 2023; Favaro et al., 2017; Fügenschuh et al., 1997; Laubscher, 1971; Linzer et al., 2002; Mancktelow et al., 2001; McPhee & Handy, 2024; Pennacchioni & Mancktelow, 2013; Scharf et al., 2013; Schmid & Kissling, 2000; Schmid et al., 1996, 2013; Verwater et al., 2021; Villani et al., 2024) and a huge amount of geological and structural data were gained in the course of the tunnel construction (Brandner et al., 2008b; Töchterle et al., 2007). However, penetrative deformation arising from contemporaneous N-Sshortening and orogen-parallel extension, coupled with the limited data regarding the extent of lateral movement and the lack of stratigraphic markers within the core of the western TW, renders conventional cross-section balancing impossible. We therefore constrain our model with fission-track data (compilation of Bertrand et al., 2017; Most, 2003) and with information from temperature-time- and temperature-depth paths (Fügenschuh et al., 1997; von Blanckenburg et al., 1989). To restore the nappes of the western TW to the pre-indenter stage, we use unfolding and movement along the Sub-Tauern ramp (Ortner et al., 2006; Reiter et al., 2018; TRANSALP Working Group et al., 2002).

# 2. Tectonic Setting

# 2.1. Structural Overview

# 2.1.1. Subpenninic Nappe System

The core of the Subpenninic nappe system (and of the western TW) consists of the Venediger nappe system (e.g., Frisch, 1977; Lammerer & Weger, 1998; Lammerer et al., 2008; Schmid et al., 2013). The duplex structure of which was first deciphered by Lammerer and Weger (1998). Three main gneiss cores can be distinguished in map view (Figure 1b; Frisch, 1977): From north to south, the Ahorn gneiss core (AGC) is the structurally lowest duplex horse, which is overthrusted by the Tuxer gneiss core (TGC). The upper- and southernmost horse of the duplex is the Zillertaler gneiss core (ZGC). According to the TRANSALP seismic section interpretation of Lammerer et al. (2008), a fourth horse is suspected below the AGC, which we term the Sub-Tauern gneiss core (STGC) in this work (Figure 1c; see also Brandner, 2013; Eizenhöfer et al., 2023; Ortner et al., 2006; Reiter

Figure 1. (a) Tectonic map of the Eastern Alps (modified after Rosenberg et al., 2015; Schmid et al., 2004). (b) Tectonic map of the western Tauern Window (for maps that we used, see "Data Availability Statement" section). The transparent boxes show the range of apatite fission-track ages (AFT) and zircon fission-track ages (ZFT) of the nappe on which they are plotted (compilation of Bertrand et al., 2017). For the spatial distribution of the aforementioned ages, we refer to Bertrand et al. (2017) as well. Black dots are ZFT sample locations (estimated from the compiled map of Bertrand et al., 2017) labeled with rounded-off ages in Ma (Most, 2003; see also Supporting Information S1 for further data information). (c) Cross-section along the Brenner Base Tunnel (modified after Brandner et al., 2008b; Reiter et al., 2018; Rosenberg & Garcia, 2011; Schmid et al., 2013; Töchterle et al., 2007). Assumed thrust faults (dashed lines) were taken from Reiter et al. (2018). Nappe system and Alpine unit abbreviations: PNS, Penninic nappe system; SA, Southalpine. Nappe abbreviations: AN, Antholtz nappe; AGC, Ahorn gneiss core; IQPN, Innbrucker Quartzphyllite nappe; ÖSN, Ötztal Stubai nappe; PN, Patscherkofel nappe; MMN, Meran Mauls nappe; SHWN, Subpenninic hanging-wall nappes; SN, Schneeberg nappe; StN, Steinach nappe; STGC, Sub-Tauern gneiss core; TGC, Tuxer gneiss core; TaN, Taufer nappe; TeN, Texel nappe; ZGC, Zillertaler gneiss core. Fault and shear zone abbreviations: AHSZ; Ahrntal shear zone; ASZ, Ahorn shear zone; BNF, Brenner normal fault; DAV, Defereggen Antholz Vals fault; GFS, Giudicarie fault system; GSZ, Greiner shear zone; IF, Inntal fault; FF, Passeier fault; SEMP, Salzach Ennstal Mariazell Puchberg fault; SMF, Sterzing Mauls fault; TSZ, Tuxer shear zones; ZSZ, Zillertaler shear zone; ZWD, Zwischenbergen Wöllatratten Drau fault.

RUDMANN ET AL. 3 of 22

et al., 2018; TRANSALP Working Group et al., 2002). Each gneiss core of the Venediger duplex (VD) contains a km-size upright fold and it is assumed that the whole nappe-stack is detached along the Sub-Tauern ramp (Figure 1c; Eizenhöfer et al., 2023; Lammerer et al., 2008; Ortner et al., 2006; Reiter et al., 2018). The gneiss cores are mainly composed of meta-plutonites, yielding ages of 335–292 Ma, which intruded into Variscandeformed basement rocks (Veselá et al., 2011 and references therein), named "Altes Dach" (Frasl, 1958) and Greiner schists (Lammerer, 1986) in the literature.

During the Carboniferous-Permian period, horst and graben structures developed in the Alpine area as a result of Late to Post-Variscan extensional tectonics (e.g., von Raumer, 1998). According to Veselá et al. (2008), Veselá and Lammerer (2008), and Veselá et al. (2022), the AGC, TGC, and ZGC represent former horst blocks, which were separated once by the Riffler-Schönach basin (between AGC and TCG) and the Pfitsch-Mörchner basin (between TGC and ZGC). Sediments and some volcanites filled these basins, probably until the Mid-Mesozoic (Veselá et al., 2008, 2011, 2022). Beginning in the Early Jurassic, the entire Tauern region became increasingly marine, which led to sedimentary deposition directly on top of the horsts ("Hochstegenzone"; Frisch, 1974).

Today, these Jurassic units build, as an autochthonous nappe, the uppermost part of the VD and are internally in part isoclinally folded (e.g., Frisch, 1974; Schmid et al., 2013), while the former basins are strongly deformed and squeezed between the gneiss cores (e.g., Veselá & Lammerer, 2008; Veselá et al., 2008).

The VD was overthrusted by Subpenninic, Permo-Mesozoic nappes, which can partly be ascribed to the Upper "Hochstegenzone" based on similarities, which is why their amount of displacement are suspected to be just a few kilometres (e.g., Frisch, 1974). The separation and classification of these nappes, which mainly depends on the age of the "Kaserer-Series", have been a matter of debate since decades (Brandner et al., 2008a; Frisch, 1974, 1980; Lammerer, 1986; Lammerer et al., 2008; Rockenschaub et al., 2003; Thiele, 1980; Töchterle, 2011; Töchterle et al., 2011; Veselá & Lammerer, 2008; Veselá et al., 2022). In this work, we name them "Subpenninic hanging-wall nappes of the VD" and ascribe them to the VD s. lat. These nappes include the "Wolfendorn nappe" (Frisch, 1974), "Kaserer nappe" (Veselá et al., 2022) and "Flatschspitz nappe" (Brandner et al., 2008a; Töchterle, 2011). In the last decades, the "Modereck nappe system" (Schmid et al., 2013) was ascribed to these hanging-wall nappes as well, in particular in the central TW (Groß et al., 2020, 2021, 2022), as the structurally uppermost nappe is mainly composed of (Permo-)Triassic units (e.g., Rockenschaub et al., 2003; Schmid et al., 2013 and references therein). However, in the course of the Brenner Base Tunnel construction, no evidence was found for a tectonic contact with the overlaying Glockner nappe system in the western TW (Brandner et al., 2008a, 2008b; Töchterle, 2011; Töchterle et al., 2007, 2011). For this reason, we use the term "Triassic succession at the base of the Glocker nappe system," as already proposed by Frisch (1974).

### 2.1.2. Penninic Nappe System

The next higher structural layer above the Subpenninic nappe system is the Penninic nappe system (Figure 1), which comprises deformed and metamorphosed oceanic sequences related to the Penninic Ocean. The base of the Lower Penninic nappe system (Glockner nappe, after Staub, 1924) form (Permo-)Triassic units that were deposited on the European shelf and are overlaid by alternating calcareous-rich, calcareous-poor and calcareous-less schists ("Bündnerschiefer" in Glockner facies; Frasl & Frank, 1966) as well as ophiolites (e.g., Höck & Koller, 1989; Koller & Prestal, 2003; Rockenschaub et al., 2003 and references therein; Schmid et al., 2013). The Upper Penninic nappe system ("Matrei Nordrahmen zone"; Rockenschaub et al., 2003 and references therein), in addition, is characterized by the appearance of Lower Austroalpine lenses. This zone constitutes the tectonic frame of the TW to the overlaying Austroalpine nappe system and is therefore regarded as a tectonic mélange zone (e.g., Brandner et al., 2008b; Koller & Prestal, 2003; Rockenschaub et al., 2003 and references therein; Töchterle et al., 2007).

In cross-section view, the Penninic nappe system traces the underlying antiform produced by the Subpenninic nappe system (Figure 1c; see also Brandner, 2013; Brandner et al., 2008b; Töchterle et al., 2007). The northern limb dips with ca. 20–30° toward the north. Its southern limb dips almost vertically and in the westernmost TW, it is even overturned. Its thickness, however, strongly decreases from north to south. In the cross-section of Reiter et al. (2018), the northern limb of the Penninic nappe system has a thickness of roughly 7 km, which completely thins out at 12 km depth, south of the ZGC (Figures 1c and 2).

RUDMANN ET AL. 4 of 22

onlinelibrary.wiley.com/doi/10.1029/2024TC008371 by Martin Luther University Halle-Wittenberg, Wiley Online Library on [16/10/2025]. See the Terms and Condit

conditions) on Wiley Online Library for rules of

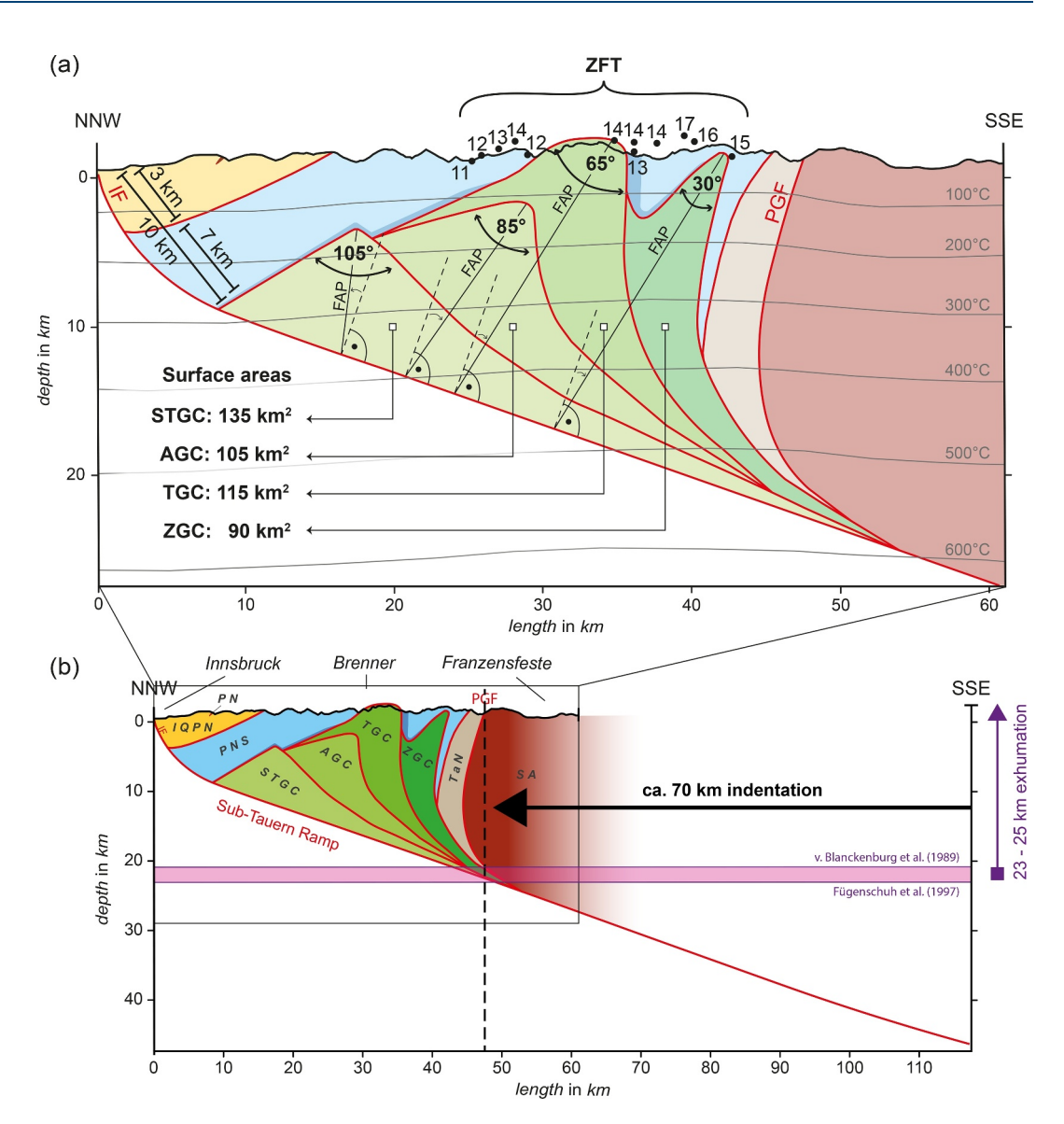


Figure 2. (a) Simplified cross-section through the western Tauern Window along the trace of the Brenner Base Tunnel, based on published cross-sections (see "Data Availability Statement" section). Black dots are projected sample locations of zircon fission-track (ZFT) data (Figure 1b). Black numbers are ZFT ages (Most, 2003; see also Supporting Information S1 for further data information). Present-day isotherms were taken from Eizenhöfer et al. (2023). For further description, see text. (b) Pre-indenter depth of the top of the Venediger duplex is indicated by the purple zone (derived from Fügenschuh et al., 1997; von Blanckenburg et al., 1989). 70 km shortening is derived by the offset of the Periadriatic fault system along the Giudicarie fault system. The dashed line represents the position where the Pustertal Gailtal fault, the eastern segment of the Periadriatic fault system, outcrops at the surface. Abbreviations: AGC, Ahorn gneiss core; FAP, Fold axial plane; IQPN, Innsbrucker Quartzphyllite nappe; PGF, Pusteral Gailtal fault; PN, Patscherkofel nappe; PNS, Penninic nappe system; SA, Southalpine; STGC, Subtauern gneiss core; TaN, Taufer nappe; TGC, Tuxer gneiss core; ZGC, Zillertaler gneiss core.

# 2.1.3. Austroalpine Nappe System

The Austroalpine nappe system overlays and thus, in map view, frames the TW as the structurally uppermost layer (Figure 1). It is a complex nappe system that was assembled during the Cretaceous Eoalpine event (e.g., Foitzheim et al., 1994). Following Schmid et al. (2004), the Austroalpine nappe system can be subdivided into the Lower and Upper Austroalpine nappe system. Units of the Lower Austroalpine nappe system are derived from a highly distal or external area of the former northern passive continental margin of the Adriatic plate, whereas the Upper Austroalpine nappe system units have an intracontinental origin (Schmid et al., 2004 and references therein). In

RUDMANN ET AL. 5 of 22

the following, we focus only on the Upper Austroalpine basement nappes, based on the definition of Schmid et al. (2004, 2013) and references therein, as the Lower Austroalpine nappe system is present only as slivers.

Following the classification of Schmid et al. (2013), from structural lowest to highest, the basement nappes that are attributed to the Austroalpine nappe systems are as follows (see also Figure 1b):

- Silvretta Seckau nappe system: Innsbrucker Quartzphyllite nappe.
- Koralpe Wölz nappe system: Schneeberg nappe, Taufers nappe, Texel nappe.
- Ötztal Bundschuh nappe system: Ötztal Stubai nappe, Patscherkofel nappe.
- Drauzug Gurktal nappe system: Antholtz nappe, Meran Mauls nappe, Steinach nappe.

# 2.1.4. Eastern Southern Alps (Dolomites Indenter)

To the south, the Austroalpine nappe system is juxtaposed against the Southalpine units along the Periadriatic fault system, one of the major fault systems in the Alps. The Giudicarie fault system (the central NNE-SSW striking part of the Periadriatic fault system) divides the Southalpine into eastern (Dolomites indenter; Rosenberg et al., 2007) and western (Insubric or western Alpine indenter; Rosenberg et al., 2007) parts from the Late Oligocene on (Pomella et al., 2011, 2012; Verwater et al., 2021). The Dolomites indenter consists of Variscan deformed and metamorphosed Neoproterozoic to Cambrian basement and its post-Variscan volcanic and sedimentary cover. The basement was intruded by Permian granite and granodiorite, now exposed predominantly along the western and northern boundary of the Dolomites indenter.

### 2.1.5. Relevant Faults and Shear-Zones

The western TW is traversed by several SW-NE-striking, steeply dipping, large-scale shear zones (Figures 1a and 1b), which were active between ca. 33-7 Ma (Schneider et al., 2013 and references therein). Based on Schneider et al. (2013), the most important ones are, from north to south, the Ahorn shear zone, the Tuxer shear zones, the Greiner shear zone and the Ahrntal shear zone (Figures 1a and 1b). All of them are mylonitic shear zones, partly overprinted by brittle deformation (e.g., Behrmann & Frisch, 1990; Berryman et al., 2017; Pennacchioni & Mancktelow, 2013) and show predominant sinistral-transpressive kinematics (e.g., Behrmann & Frisch, 1990; Reicherter et al., 1993; Rosenberg & Schneider, 2008; Schneider et al., 2013). In addition, minor dextral kinematic indicators could be observed in the Greiner shear zone and the Ahrntal shear zone (e.g., Barnes et al., 2004; Schneider, 2015). The Ahorn shear zone runs along the northern border of the AGC, the Tuxer shear zones dissects the TGC and the Greiner shear zone runs through the Pfitsch-Mörchner basin (Schneider et al., 2013; Figure 1b). The ZGC is cross-cut by shear zones, too, as observed by Pennacchioni and Mancktelow (2007). We summarize these as the Zillertaler shear zones (Figure 1b). The Ahrntal shear zone runs along the southern border of the Penninic nappe system and Austroalpine nappe system, then passes the Penninic nappe system on its eastern course until it finally turns into the boundary of the Subpenninic nappe system and Penninic nappe system (Schneider et al., 2013; Figure 1b). It has been proposed that the continuations of these shear zones merge into the sinistral-transpressive SEMP to the east (Figure 1a; e.g., Lammerer et al., 2008; Linzer et al., 2002; Rosenberg & Schneider, 2008).

The BNF delimitates the western TW to the west (e.g., Axen et al., 1995; Behrmann, 1988; Fügenschuh et al., 1997, 2012; Rosenberg & Garcia, 2011, 2012; Selverstone, 1988). It is a large-scale, low-angle normal fault that dips toward the west and has both viscous and brittle components. The viscous segment can be traced between Steinach and Sterzing. This mylonitic shear zone is several km thick and is overprinted by brittle normal faults, which dip steeper to the west than the mylonitic shear zone. In the segment between Steinach and Innsbruck (Silltal fault after Schmidegg, 1954, or Wipptal fault after Reiter et al., 2003), only brittle deformation has been observed.

The Defereggen Antholz Vals fault separates nappes of the Koralpe Wölz nappe system and Drauzug Gurktal nappe system (Figures 1a and 1b; Schmid et al., 2013). It is a Cretaceous, mylonitic, former top-to-SE, down-faulting shear zone, which has been steepened, in the research area even overturned, and reactivated as a sinistral strike-slip fault during indentation of the eastern Southern Alps (Borsi et al., 1973; Mancktelow et al., 2001). In the southwestern corner of the TW, the Defereggen Antholz Vals fault comes very close to the tip of the Dolomites indenter (Figures 1a and 1b) creating a tectonically very complex area (Bistacchi et al., 2010; Klotz et al., 2019; Massironi et al., 2011).

RUDMANN ET AL. 6 of 22

AGU

ADVANCING EARTH
AND SPACE SCIENCE

The Periadriatic fault system is defined as the northern boundary of the Southalpine (e.g., Schmid et al., 1989). Specifically, the Dolomites indenter is bounded to the west and northwest by the sinistral Giudicarie fault system

10.1029/2024TC008371

(including the NNE-SSW-striking southern and northern Giudicarie fault and the SW-NE-striking, top-to-SE-thrusting Meran Mauls fault) and to the north by the dextral, WNW-ESE-striking Pustertal Gailtal fault (Figure 1b; e.g., Pomella et al., 2011, 2012; Schmid et al., 2004). A detailed description of the evolution of the Periadriatic fault system is given in the second paragraph of the following section "Tectonic history."

# 2.2. Tectonic History

The TW has been the focus of research over the last decades (see Rosenberg et al., 2018; Schmid et al., 2013 for reviews), whereby different theories about its formation, including various deformation phases were postulated. We follow the division of the deformation phases of Schmid et al. (2013; D1–D5), being fully aware that alternatively-inferred deformation phases exist (see compilation in Rosenberg & Schneider, 2008). We distinguish between pre-indenter (D1–D4; subduction and closure of the Penninic Ocean, nappe-stacking and VD formation) and indenter phase (D5; upright folding of the western TW, W-E extension, which includes orogen-perpendicular normal faults and lateral extrusion toward the east). In the following, we concentrate on the latter deformation phase.

In our tectonic model, we assume an originally straight Periadriatic fault system, based on the works of for example, Laubscher (1971), Pomella et al. (2012), Ratschbacher, Merle, et al. (1991), Ratschbacher, Frisch, et al. (1991), Schmid and Kissling (2000), Schönborn (1992), and Stipp et al. (2004). The synkinematically intruded plutonites (Periadriatic intrusions; e.g., Pomella et al., 2011; Rosenberg, 2004; Stipp et al., 2004) date this phase to at least the Middle Oligocene. According to the three-phase deformation model of Pomella et al. (2012), the onset of indentation likely occurred during the Late Oligocene or Earliest Miocene, resulting in the bending of the formerly straight, E-W-striking Periadriatic fault system. As a consequence, the northeastern part of the Adamello pluton (Periadriatic intrusion) was dragged in a northeastern direction. Today, this phase is manifested by the viscous part of the Meran Mauls fault and the occurrence of a thin but continuous tonalitic lamella (Periadriatic intrusion) along this fault (Pomella et al., 2011). In Late Oligocene/Early Miocene (Pomella et al., 2011, 2012), no later than 21 Ma (e.g., Scharf et al., 2013; Schmid et al., 2013, and references therein), a progressive northward push of the Dolomites indenter caused the Giudicarie fault system to cross-cut the previously-bent Periadriatic fault system (i.e., the Meran Mauls fault). The offset reached 75 km until present-day (Favaro et al., 2017 and references therein; Verwater et al., 2021), which corresponds to ca. 70 km northward displacement (Figure 1a).

The strong N-S-shortening of ca. 70 km, resolved north of the tip of the Dolomites indenter (corresponding to the offset of the Periadriatic fault system along the Giudicarie fault system; Figure 1a), caused coeval doming, formation of orogen-perpendicular normal faults and lateral extrusion toward the east (e.g., Favaro et al., 2017; Ratschbacher, Frisch, et al., 1991; Ratschbacher, Merle, et al., 1991; Ricchi et al., 2020; Scharf et al., 2013, Schmid et al., 2013 and references therein), whereby the western TW was vertically exhumed by 23–25 km (von Blanckenburg et al., 1989; Fügenschuh et al., 1997, respectively). According to the retro-deformation of the TRANSALP cross-section by Lammerer et al. (2008), exhumation of the AGC, TGC, and ZGC together was caused by viscous folding and displacement along a blind thrust at the base of the AGC between 30 and 20 Ma, which caused a 13 km-high duplex structure. When folding locked, displacement was localized along the Sub-Tauern ramp, which generated the STGC by up-ramping. After Lammerer et al. (2008), the latter phase took place between 20 and 10 Ma and resulted in 17 km northward slip along the Sub-Tauern ramp and 8 km vertical exhumation. Thermochronological data of Fügenschuh et al. (1997) reveal that exhumation was fastest between ca. 20 and 18 Ma (4 mm/a), it decreased to 2.6 mm/a until ca. 15 Ma, slowed down to 1 mm/a until 10 Ma, and then it reduced to ≤0.2 mm/a until present-day. Bertrand et al. (2017) calculated exhumation rates of ≥5 mm/a between ca. 20–10 Ma and ≤5 mm/a from 8 Ma onwards.

Wolff et al. (2020) used low-temperature thermochronology to model the onset of deformation ( $19 \pm 2$  Ma) on the BNF in the Brenner Pass area. According to their model, the activity of the BNF terminated at ca. 9 Ma and erosion dominated. This is in line with Fügenschuh et al. (1997), who postulate the onset of the BNF at ca. 20 Ma and the decrease of the exhumation rate to 0.2 mm/a between 10 Ma and present-day, as mentioned above. However, Fügenschuh et al. (1997, 2012) assume that the viscous part of the BNF acted together with the northern and southern margin of the TW (Tauern northern boundary and Sterzing Mauls fault, respectively) as a down-

RUDMANN ET AL. 7 of 22

faulting envelope during the early phase of indentation (see also Töchterle et al., 2011). Thus, the Silltal fault, the northern brittle segment of the BNF, developed in a later stage, as VD, Penninic nappe system and Innsbrucker Quartzphyllite nappe exhumed together along this fault (from ca. 13 Ma on). In contrast, Rosenberg et al. (2018) and references therein propose that the transition from the viscous BNF to the brittle Silltal fault could represent the Miocene brittle-ductile transition of the BNF, which was exhumed and tilted northwards along strike during updoming of the TW. In addition to the discussion about the trend of the fault, the amount of horizontal extension on the BNF is a matter of debate. The published values range from 50 to >70 km (Fügenschuh et al., 1997), 33– 63 km (Axen et al., 1995), 44 km (Fügenschuh et al., 2012) and  $35 \pm 10$  km (Wolff et al., 2020) to 2–14 km (Rosenberg & Garcia, 2011, 2012).

Lateral extrusion toward the east occurred along major strike-slip faults such as the Inntal fault, the SEMP, the Mölltal fault and the Pustertal Gailtal fault (peak of activity between 19 and 10 Ma; e.g., Ricchi et al., 2020), whereby the amount of displacement increases in an eastern direction (e.g., Linzer et al., 2002; Ratschbacher, Frisch, et al., 1991; Ratschbacher, Merle, et al., 1991; Rosenberg et al., 2007; Scharf et al., 2013). The total amount of lateral escape ranges between ca. 170 km (Frisch et al., 1998) or 120 km (Linzer et al., 2002) to around 75 km (Favaro et al., 2017; Rosenberg et al., 2007; see also discussion in Rosenberg et al., 2018). However, in the western TW, it is assumed that the amount of lateral displacement approaches zero, and lateral motion was accommodated by folding (e.g., Rosenberg & Schneider, 2008; Töchterle et al., 2011).

### 3. Database and Methods

For our kinematic restoration, we compiled and simplified a geological cross-section of the western TW along the trace of the Brenner Base Tunnel (based on several cross-sections through the western TW, see "Data Availability Statement" section). We used the cross-section along this trace for two reasons: (a) It is oriented approximately perpendicular to the fold axes of the upright folds of the TW and therefore parallel to the tectonic transport direction during the Miocene (e.g., Eizenhöfer et al., 2023; Favaro et al., 2017; Fügenschuh et al., 1997; Laubscher, 1971; Linzer et al., 2002; Mancktelow et al., 2001; McPhee & Handy, 2024; Pennacchioni & Mancktelow, 2013; Scharf et al., 2013; Schmid & Kissling, 2000; Schmid et al., 1996, 2013; Verwater et al., 2021; Villani et al., 2024). (b) A huge amount of geological and structural data was gained in the course of the construction of the Brenner Base Tunnel (Brandner et al., 2008b; Töchterle et al., 2007). Töchterle et al. (2007) present a cross-section in which the aforementioned data are included, which is therefore wellconstrained, at least for the upper ca. 2 km. The cross-section of Reiter et al. (2018) covers the deep structure as well (up to 35 km depth; Figure 1c), although not as well-constrained as the upper ca. 2 km and therefore in parts speculative. Their cross-section is based on Brandner et al. (2008b), Brandner (2013), and Ortner et al. (2006), and on reflectors visible in the TRANSALP seismic section (TRANSALP Working Group et al., 2002; Figures 1a and 1b), in particular for information about the Sub-Tauern ramp (we refer to their publication for more details). For our retrodeformation, we simplified the cross-section of Töchterle et al. (2007) and Reiter et al. (2018) (Figure 2a). It comprises the VD, including its Subpenninic hanging-wall nappes (green units), the Penninic nappe system (blue unit), the Innsbrucker Quartzphyllite nappe (vellow unit), the Koralpe Wölz nappe system (light brown unit), and the Southalpine (red-brown unit) (Figure 2). Structural analysis of the VD reveals surface areas of the gneiss cores of ca. 135 km<sup>2</sup> (STGC), 105 km<sup>2</sup> (AGC), 115 km<sup>2</sup> (TGC) and 90 km<sup>2</sup> (ZGC), respectively (Figure 2a). The interlimb angles of the gneiss cores decrease in southern direction (STGC: 105°, AGC: 85°, TGC: 65°, ZGC: 30°; Figure 2a). Fold axial planes of the AGC, the TGC and the ZGC are slightly south-vergent (ca. 10–15°), with respect to the Sub-Tauern ramp (Figure 2a). In the model, we consider fold axial planes to be geometrical constructs (pins) and not mechanical boundaries.

The Sub-Tauern ramp dips ca. 20° to the south, and steepens toward and emerges in the Inn Valley. Further descriptive values (e.g., thicknesses of the hanging-wall nappes and inclinations of fold limbs) are given in Section 2.1.2.

2-D kinematic restoration of the VD was carried out with the software MOVE<sup>TM</sup> version 2019.1 (petroleum experts).

Over the last decades, retro-deformation techniques have been used to quantify the amount of horizontal shortening of fold-and-thrust belts (e.g., Dahlstrom, 1969; De Paor, 1988; Jourdon et al., 2014; McPhee et al., 2018; Schönborn, 1999) and sedimentary basins (e.g., Brandes et al., 2013; Coward, 1996). These techniques require that all rigid-body deformation and strain that evolve in a rock volume are controlled by geometric

RUDMANN ET AL. 8 of 22

19449194, 2025, 7, Downloaded from https://agupubs.onlinelibrary.wiley.com/doi/10.1029/2024TC008371 by Martin Luther University Halle-Wittenberg, Wiley Online Library on [16/10/2025]. See the Terms and Conc

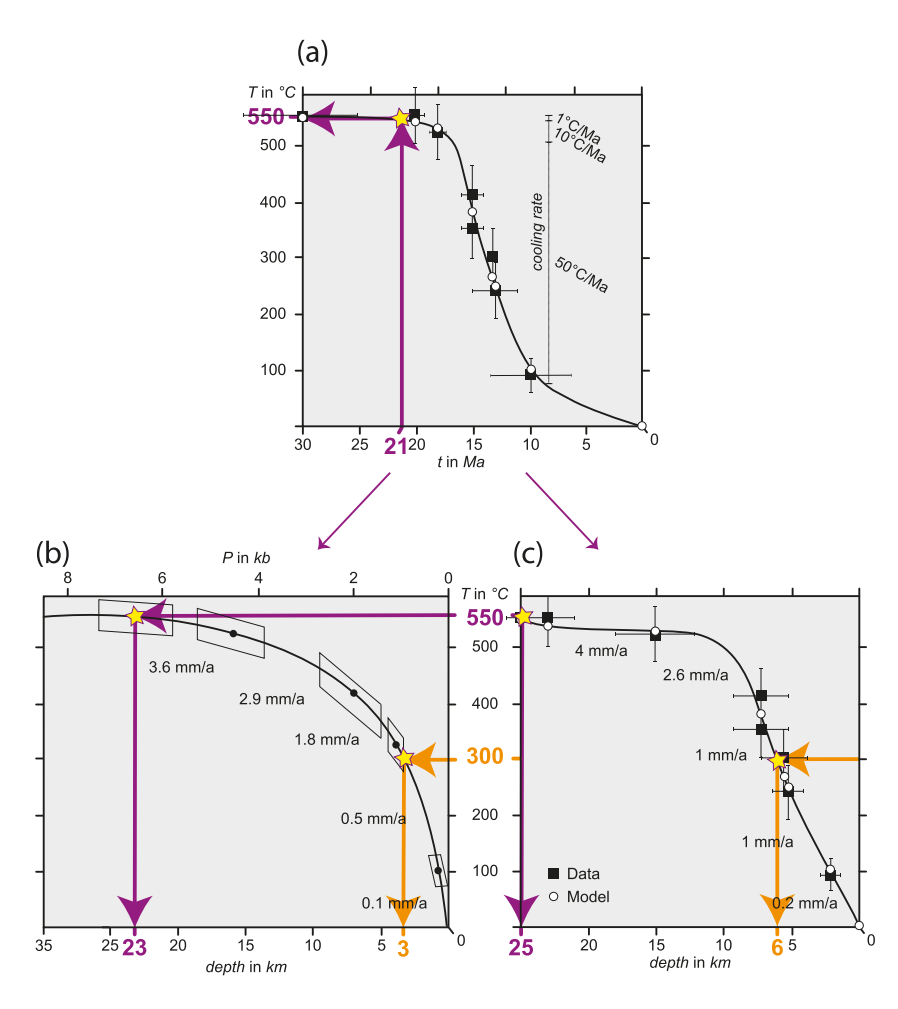


**Figure 3.** (a) Temperature-time path of Fügenschuh et al. (1997). The purple arrows show the temperature conditions (550°C) of the top of the Venediger duplex (VD) at 21 Ma (latest onset of the activity of the Giudicarie fault system; Schmid et al., 2013 and references therein). Changing cooling rates during exhumation are indicated along the curve. Temperature-depth path of (b) von Blanckenburg et al. (1989), and (c) Fügenschuh et al. (1997). Purple arrows point to the pre-indenter depth at which the top of the VD was located at temperature conditions of 550°C, which is (b) 23 km, and (c) 25 km b.s.l. Orange arrows point to the depth in which 300°C prevailed, which is 3 km (a) and 6 km (c).

laws. Valid restorations require that (a) the analyzed structures display reasonable natural geometries, (b) the geometry after retro-deformation must be reasonable, (c) mass must be conserved and (d) the kinematic development from the undeformed to the deformed state must be physically possible (Marshak & Wilkerson, 2004; Wilkerson & Dicken, 2001). However, standard cross-section balancing of a cross-section through the western TW is not possible, because (a) standard assumptions, such as plane-strain conditions (Woodward et al., 1989) cannot be made and, (b) in contrast to structural restoration of deformed sedimentary basin-fills or thin-skinned foreland fold-and-thrust belts (e.g., Balling et al., 2021; Brandes et al., 2016; Tanner et al., 2003), no stratigraphic markers exist for the VD, and the Subpenninic hanging-wall nappes were already displaced at pre-indenter stage. We therefore used other constraints:

Zircon fission-track (ZFT) ages ( $11 \pm 1.4$ – $17 \pm 0.6$  Ma; Most, 2003) were used as an approximation of a conservative time constraint for the termination of viscous folding of the VD, that is at the point of time of the ZFT ages folding is definitely inactive. The VD has a felsic composition with a high quartz content, which means that viscous folding must have taken place at temperatures above ca. 270–310°C (brittle to viscous transition of quartz, assuming a slow natural strain rate; cf. van Daalen et al., 1999; Stöckhert et al., 1999; Stipp et al., 2002b); we take 300°C as a mean value. After Brandon et al. (1998) and Reiners and Brandon (2006), the partial annealing zone of ZFT strongly depends on the cooling rate, whereby higher cooling rates shift the zone to higher temperatures. The temperature-time path of Fügenschuh et al. (1997) shows a cooling rate of ca. 10°C/Ma between the latest onset of

RUDMANN ET AL. 9 of 22

indentation (21 Ma) and the oldest ZFT cooling age in our model ( $17 \pm 0.6$  Ma) (Figure 3a). This is equivalent to a partial annealing zone of 205–265°C (with a mean closure temperature of 235°C; Brandon et al., 1998; Reiners & Brandon, 2006). Between 17 and 9 Ma, the cooling rate increased to 50°C/Ma (Fügenschuh et al., 1997; Figure 3a), which corresponds to a ZFT partial annealing zone of 220–280°C (mean closure temperature of 250°C; Brandon et al., 1998; Reiners & Brandon, 2006), and is thus closer to the brittle-viscous transition.

ZFT data of the VD are sparse in the direct vicinity of our cross-section and those that do exist are most likely geothermally affected by the BNF (Wolff et al., 2020). In addition, former sampling campaigns focused on the TRANSALP transect, where geophysical data are available, and the orthogneisses are also exposed over a larger area than in the Brenner area (e.g., Eizenhöfer et al., 2021, 2023). For our kinematic restoration, we therefore projected ZFT data from ca. 25 km further east (Figure 1b) horizontally with 248°N azimuth (mean strike of the fold axes of the VD) onto our cross-section plane (Figure 2). ZFT ages range between 11  $\pm$  1.4 Ma in the north (AGC) to 17  $\pm$  0.6 Ma in the south (ZGC) (all ages given with  $1\sigma$  errors; Most, 2003; Figures 1b and 2; see also Table S1 in Supporting Information S1).

In the first part of our restoration, we displaced the entire VD down along the Sub-Tauern ramp, until the oldest ZFT cooling age ( $17 \pm 0.6$  Ma) was placed below (a) the ZFT annealing zone and (b) the 300°C isotherm. These depths strongly depend on the geothermal gradient and the starting elevation a.s.l. We assume a constant topographic elevation of 2 km a.s.l. during the Miocene, because new findings suggest that the topographic elevation of the Eastern Alps during that time span did not change significantly (Ballian et al., 2024). In addition, we tested different geothermal gradients ( $30^{\circ}$ C/km (present-day), 50 and  $70^{\circ}$ C/km) and compared our models with previous studies (Eizenhöfer et al., 2023; Fügenschuh et al., 1997; von Blanckenburg et al., 1989; Wolff et al., 2020). In the following, we present the most realistic models (30 and  $50^{\circ}$ C/km; see also Figure S1 in Supporting Information S1 for an unrealistic model of  $70^{\circ}$ C/km). The present-day isotherms were taken from Eizenhöfer et al. (2023; Figure 2).

To define the maximum depth (pre-indenter depth) at which the top of the VD was located at 21 Ma (at the latest onset of activity of the Giudicarie fault system; Schmid et al., 2013 and references therein), we used temperature-time- and temperature-depth paths of Fügenschuh et al. (1997) and von Blanckenburg et al. (1989). According to these studies, the top of the VD reached temperature conditions of 550°C at 21 Ma (Figure 3a). This temperature corresponds to 23 km depth (von Blanckenburg et al., 1989; Figure 3b), and 25 km depth (Fügenschuh et al., 1997; Figure 3c), respectively, starting at sea level. Assuming a constant elevation of 2 km a.s.l during the Miocene, this maximum depth shifts 2 km upwards, resulting in ca. 21–23 km b.s.l.

For the retro-deformation in the viscous regime, we use unfolding algorithms. We choose to preserve the surface area, because we do not know how much material was transported out of the cross-section plane by orogen-parallel normal faulting and lateral extrusion toward the east, or whether material left the cross-section plane at all. Area balancing is therefore the minimum criteria for our restoration, because any material that was transported out of the cross-section plane would increase the cross-sectional area backwards in time. We unfolded each gneiss core individually, because we assume that they were originally (pre-indenter) symmetrical duplex horses, each having the same interlimb angle, and that their fold axial planes were oriented perpendicular to the Sub-Tauern ramp (based on Boyer & Elliott, 1982). We tested two scenarios: (a) Only unfolding and (b) unfolding during continuous slip along the Sub-Tauern ramp.

Finally, we reconstructed the northern limbs of the hanging-wall nappes (Penninic nappe system and Innsbrucker Quartzphyllite nappe; Figure 2) on top of the finished restoration of the VD. We can precisely constrain the position of the present-day outcrop surface of the Innsbrucker Quartzphyllite nappe. This probably approximates the top of this unit, because remnants of the overlaying Ötztal Bundschuh nappe system (Patscherkofel nappe, Figure 1b) can be found at some peaks (e.g., Patscherkofel). This surface must have reached thermal conditions between the lower limit of the partial annealing zone of apatite fission-tracks (AFT), and the upper limit of the partial annealing zone of ZFT, as only the first system was reset in the Miocene (see compilation in Bertrand et al., 2017 and Figure 1b). The temperatures reached during the Neoalpine orogenesis were not high enough to reset ZFT of the Innsbrucker Quartzphyllite (ZFT ages of 70 to 41 Ma in our map section, Figure 1). In contrast, ZFT data of the Austroalpine nappes south of the VD were reset (e.g., Klotz et al., 2019; Luth & Willingshofer, 2008), meaning that they must have been positioned below the partial annealing zone of ZFT before the onset of indentation.

RUDMANN ET AL. 10 of 22

19449194, 2025, 7, Downloaded from https://agupubs.onlinelibrary.wiley.com/doi/10.1029/2024TC008371 by Martin Luther University Halle-Wittenberg, Wiley Online Library on [16/10/2025]. See the Terms and Conditions (https://agupubs.onlinelibrary.wiley.com/doi/10.1029/2024TC008371 by Martin Luther University Halle-Wittenberg, Wiley Online Library on [16/10/2025]. See the Terms and Conditions (https://agupubs.onlinelibrary.wiley.com/doi/10.1029/2024TC008371 by Martin Luther University Halle-Wittenberg, Wiley Online Library on [16/10/2025]. See the Terms and Conditions (https://agupubs.onlinelibrary.wiley.com/doi/10.1029/2024TC008371 by Martin Luther University Halle-Wittenberg, Wiley Online Library on [16/10/2025]. See the Terms and Conditions (https://agupubs.onlinelibrary.wiley.com/doi/10.1029/2024TC008371 by Martin Luther University Halle-Wittenberg, Wiley Online Library on [16/10/2025]. See the Terms and Conditions (https://agupubs.com/doi/10.1029/2024TC008371 by Martin Luther University Halle-Wittenberg, Wiley Online Library on [16/10/2025]. See the Terms and Conditions (https://agupubs.com/doi/10.1029/2024TC008371 by Martin Luther University Halle-Wittenberg, Wiley Online Library on [16/10/2025]. See the Terms and Conditions (https://agupubs.com/doi/10.1029/2024TC008371 by Martin Luther University Halle-Wittenberg, Wiley Online Library on [16/10/2025]. See the Terms and Conditions (https://agupubs.com/doi/10.1029/2024TC008371 by Martin Luther University Halle-Wittenberg, Wiley Online Library on [16/10/2025]. See the Terms and Conditions (https://agupubs.com/doi/10.1029/2024TC008371 by Martin Luther University (https://agupubs.com/doi/10.1029/2024

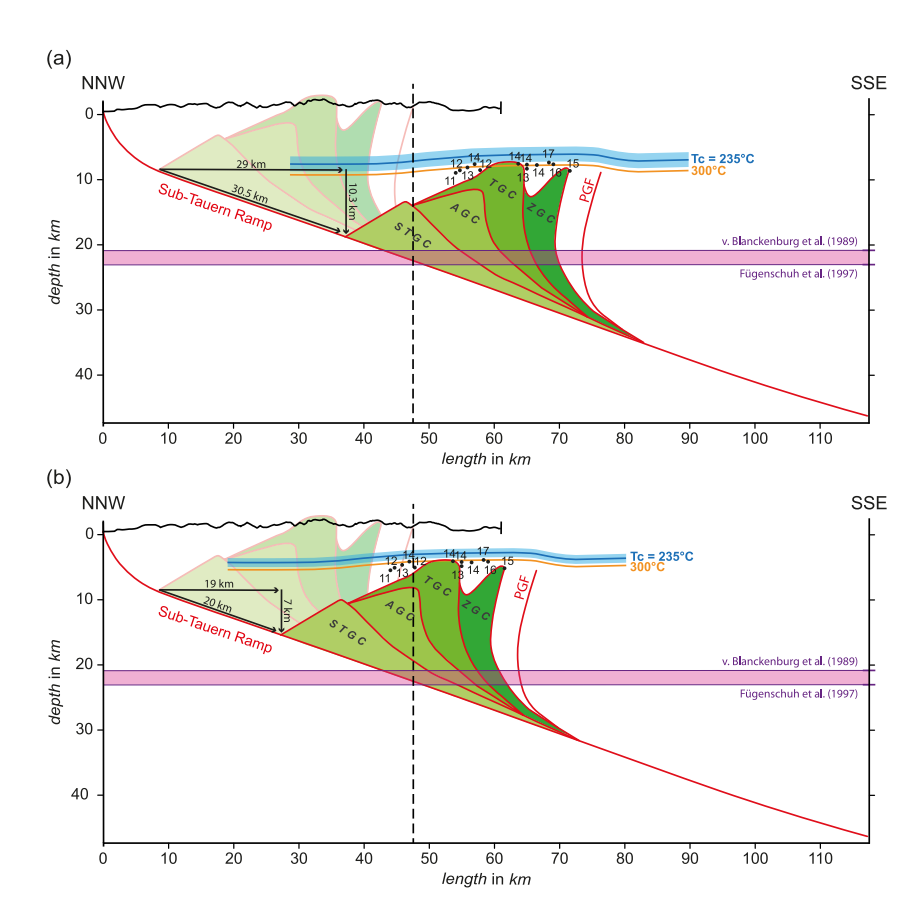


Figure 4. Displacements of the Venediger duplex (VD) along the Sub-Tauern ramp, so that zircon fission-track (ZFT) ages are below the depth of the partial annealing zone (oldest ZFT cooling age:  $17 \pm 0.6$  Ma), using a geothermal gradient of (a)  $30^{\circ}$ C/km and (b)  $50^{\circ}$ C/km. In each sub-figure, the position of the  $300^{\circ}$ C isotherm is the marker for the brittle to viscous transition for felsic rock. Pre-indenter depth of the top of the VD is indicated by the purple zone (derived from Fügenschuh et al., 1997; von Blanckenburg et al., 1989). Abbreviations: AGC, Ahorn gneiss core; PGF, Pusteral Gailtal fault; STGC, Subtauern gneiss core; TGC, Tuxer gneiss core; ZGC, Zillertaler gneiss core.

At pre-indenter stage, the cooling rate was ca. 1°C/Ma (Fügenschuh et al., 1997; Figure 3a), which means that the partial annealing zone of AFT ranges approximately between 70–130°C, with a mean closure temperature of 100°C, and of ZFT between 180–240°C with a mean closure temperature of 210°C (Brandon et al., 1998; Reiners & Brandon, 2006). The position of the partial annealing zones at depth depends on the geothermal gradient that prevailed at that time. We follow the graphs of Fügenschuh et al. (1997) (22°C/km; Figure 3c) and von Blanckenburg et al. (1989) (24°C/km; Figure 3b), and used a mean value of 23°C/km as pre-indenter geothermal gradient for our model.

We chose the boundary between the Innsbrucker Quartzphyllite nappe and the Penninic nappe system by conserving the present-day nappe thickness ratio, because we have no information on how the thicknesses of the two nappes might have changed individually. Therefore, we analyzed the total thickness of the Innsbrucker Quartzphyllite nappe and the Penninic nappe system together. The reconstruction of the remaining nappes of the Upper Austroalpine nappe system, located to the south of the western TW, is based on the tectonic model of Pomella et al. (2016), which is west and southwest of the BNF.

# 4. Results

We carried out the structural restoration of the VD in two steps: (a) down-dip transport of the VD along the Sub-Tauern ramp and (b) unfolding of the individual horses of the VD. Key temporal and spatial constraints for the restoration process are ZFT data and tectonometamorphic data sets, thus different geothermal gradients had to be tested in order to derive a most realistic deformation history from the latest onset of indentation (21 Ma) to the present-day.

RUDMANN ET AL. 11 of 22

19449194, 2025, 7, Downloaded from https://agupubs.onlinelibrary.wiley.com/doi/10.1029/2024TC008371 by Martin Lutter University Halle-Wittenberg, Wiley Onlin

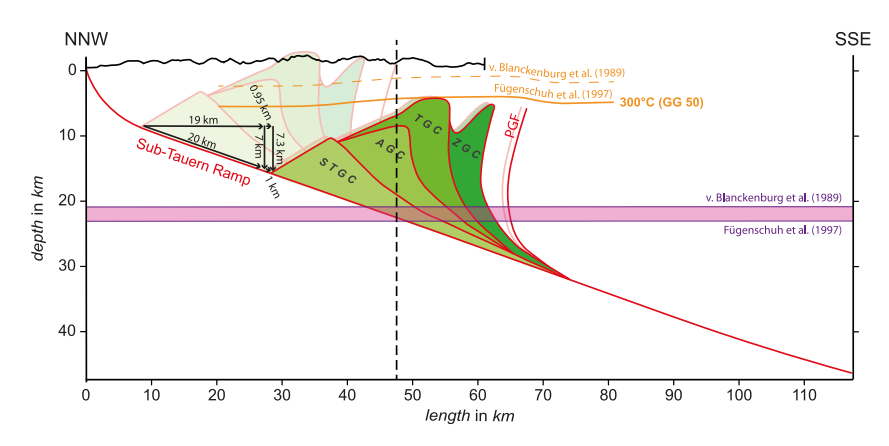


**Figure 5.** Displacement of the Venediger duplex (VD) below the 300°C isotherm of Fügenschuh et al. (1997), the depth of which corresponds to a geothermal gradient of 50°C/km. The position of the upper dashed orange 300°C isotherm is derived from the model of von Blanckenburg et al. (1989). Abbreviations: AGC, Ahorn gneiss core; PGF, Pusteral Gailtal fault; STGC, Subtauern gneiss core; TGC, Tuxer gneiss core; ZGC, Zillertaler gneiss core.

Assuming a topography with an average elevation of 2 km a.s.l., the depth at which the partial annealing zone of ZFT occurs, ranges from 4.8 to 6.8 km b.s.l. with a geothermal gradient of  $30^{\circ}$ C/km (Figure 4a), or from 2.1 to 3.3 km b.s.l. with a geothermal gradient of  $50^{\circ}$ C/km (Figure 4b). In the first case, we displace the VD by 30.5 km down along the Sub-Tauern ramp, so that the oldest ZFT cooling age that we use for our modeling ( $17 \pm 0.6$  Ma) is positioned below the partial annealing zone (Figure 4a). This corresponds to a horizontal displacement of 29 km and a vertical displacement of 10.3 km. In the case of the  $50^{\circ}$ C/km geothermal gradient, we need to displace the VD by only 20 km slip along the Sub-Tauern ramp, which corresponds to 19 km horizontal and 7 km vertical displacement (Figure 4b).

The modeled depth of the 300°C isotherm is at ca. 8 km b.s.l. (30°C/km) and ca. 4 km b.s.l. (50°C/km) including 2 km of topographic elevation (Figure 4). Comparing these depths with the temperature-depth paths of von Blanckenburg et al. (1989) and Fügenschuh et al. (1997), we find that our 50°C/km geothermal gradient model fits well with the data of Fügenschuh et al. (1997), whose model reveal 300°C in 6 km depth (Figure 3c), which corresponds to 4 km depth including 2 km topographic elevation. In contrast, the depth in which 300°C was present, derived from the model of von Blanckenburg et al. (1989), suggests 1 km b.s.l., which would correspond to a geothermal gradient of 100°C/km, which is unrealistic high (see also Figure S1 in Supporting Information S1). We therefore continue our retro-deformation process with the 50°C/km geothermal gradient model and displace the VD by another 1 km slip (equal to a further 0.95 km horizontal and 0.3 km vertical displacement) so that the entire duplex is situated below the deepest 300°C isotherm (Fügenschuh et al., 1997; Figure 5).

From this position, we then begin to unfold the felsic VD, because the environment was warm enough for viscous deformation. We unfold each gneiss core separately, so that each horse finishes with the same interlimb angle, forming a symmetrical duplex system. We consider two scenarios of how to unfold the duplex, the top of which come to rest at 21–23 km depth b.s.l., corresponding to 17 km of vertical extension:

Only unfolding (scenario 1): This scenario is based on the assumption that no displacement occurs along the Sub-Tauern ramp during upright folding (Figure 6a). Here, we had to unfold the gneiss cores by 70% (STGC), 75% (AGC), 80% (TGC), and 85% (ZGC), ending up with an initial interlimb angle of 160° for each gneiss core.

Unfolding with coeval slip along the Sub-Tauern ramp (scenario 2): The VD is further displaced by maximum 16 km slip with coeval unfolding of 60% (STGC), 65% (AGC), 70% (TGC) and 75% (ZGC). Each gneiss core ends up with an initial interlimb angle of ca. 150° (Figure 6b).

When preserving the surface area of the VD by unfolding (STGC: 135 km<sup>2</sup>, AGC: 105 km<sup>2</sup>, TGC: 115 km<sup>2</sup>, and ZGC: 90 km<sup>2</sup>), both models extend southwards by roughly 70 km.

At the time of pre-indentation, the isotherms must have been horizontal (Eizenhöfer et al., 2023). AFT and ZFT data (Figure 1b) indicate that the present day's outcropping surface of the Innsbrucker Quartzphyllite nappe must have been positioned between the partial annealing zones of AFT and ZFT at that time. This surface could also not

RUDMANN ET AL. 12 of 22

10.1029/2024TC008371

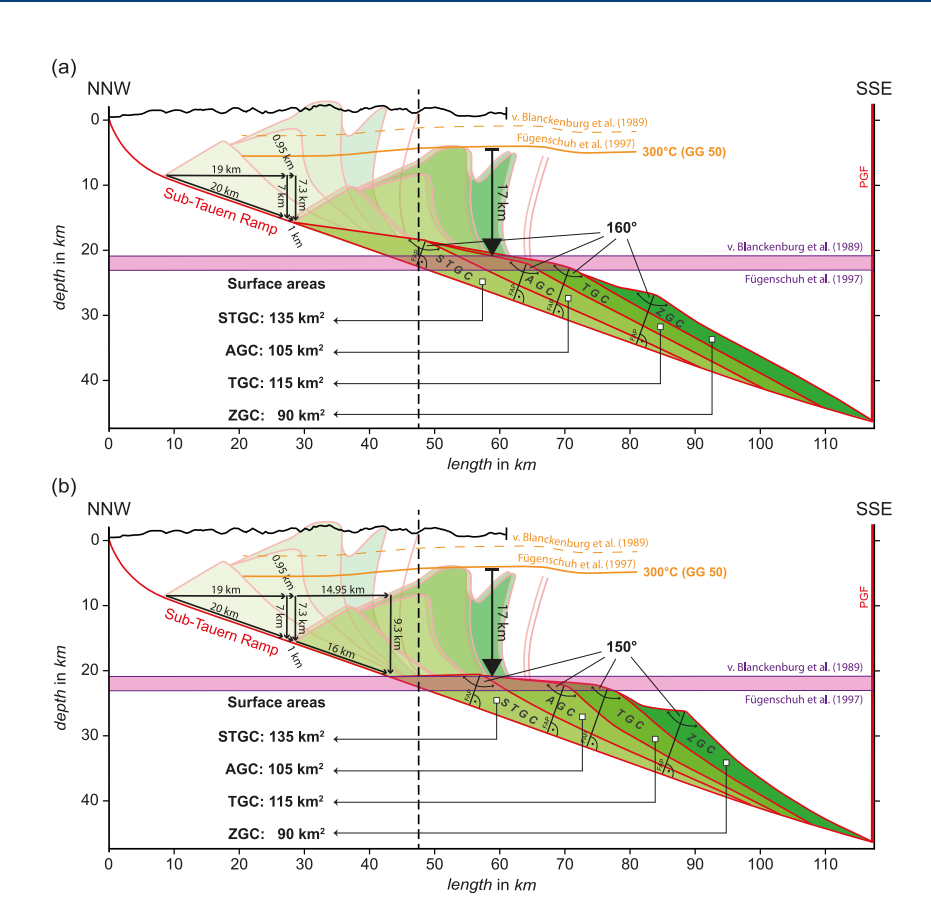


**Figure 6.** Restoration of the top Venediger duplex (VD) to 21–23 km depth (purple zone, derived from Fügenschuh et al., 1997; von Blanckenburg et al., 1989). (a) Scenario 1, only unfolding and (b) Scenario 2, unfolding during coeval slip. In both models, the trailing edge of the VD extends approximately 70 km to the south, while conserving the surface area. For further description, see text. Abbreviations: AGC, Ahorn gneiss core; PGF, Pusteral Gailtal fault; STGC, Subtauern gneiss core; TGC, Tuxer gneiss core; ZGC, Zillertaler gneiss core.

have been in a south-dipping ramp position but in an approximate horizontal position as well; otherwise, there would be Miocene ZFT ages to the south. Therefore, the present day's outcropping surface of the Innsbrucker Quartzphyllite must have been situated approximately horizontally between the partial annealing zones of AFT and ZFT (130–180°C), which is at ca. 4.75 km b.s.l., if a geothermal gradient of 23°C/km prevailed, assuming a constant elevation of 2 km a.s.l. and a cooling rate of 1°C/Ma (Brandon et al., 1998; Reiners & Brandon, 2006). We assume that the aforementioned surface represents the top of the Innsburcker Quartzphyllite, because remnants of the overlaying Ötztal Bundschuh nappe system (Patscherkofel nappe, Figure 1b) can be found at some peaks (e.g., Patscherkofel). To reach constant thicknesses of the Penninic nappe system and Upper Austroalpine nappe system in the north after restoration, the more likely scenario is scenario 2, because in our model the northern forward limb of the entire VD lies approximately horizontally as well (Figures 6b and 7). However, we cannot rule out a scenario of increasing thicknesses of the hanging-wall nappes in southern direction, because they represent the continental margin, yet we have no information about that.

If we place the top of the Innsbrucker Quartzphyllite nappe halfway between the deepest limit of the AFT partial annealing zone and the upper limit of the ZFT partial annealing zone, we find that the total thickness of the northern hanging-wall limbs together is 38% more after restoration (ca. 16.25 km) compared to the total present-day thickness of both nappes (ca. 10 km; Figures 2 and 7), using a geothermal gradient of maximum 23°C/km. If we position the top of the Innsbrucker Quartzphyllite nappe at the deepest limit of AFT partial annealing zone (3.7 km b.s.l.), the pre-indenter thickness would have even been 17.3 km. Even taking the deepest limit of the partial annealing zone of ZFT for the thickness calculation (which theoretically could also be possible), this isotherm would lie at a depth of 8.4 km. This would be in total 13.4 km pre-indenter thickness of the IQP and the PNS together, which is still 3.4 km more than today. These calculations are based on the pre-indenter depth of von

RUDMANN ET AL. 13 of 22

19449194, 2025, 7, Downloaded from https://agupubs.onlinelibrary.wiley.com/doi/10.1029/2024TC008371 by Martin Luther University Halle-Wittenberg, Wiley Online Library on [16/10/2025]. See

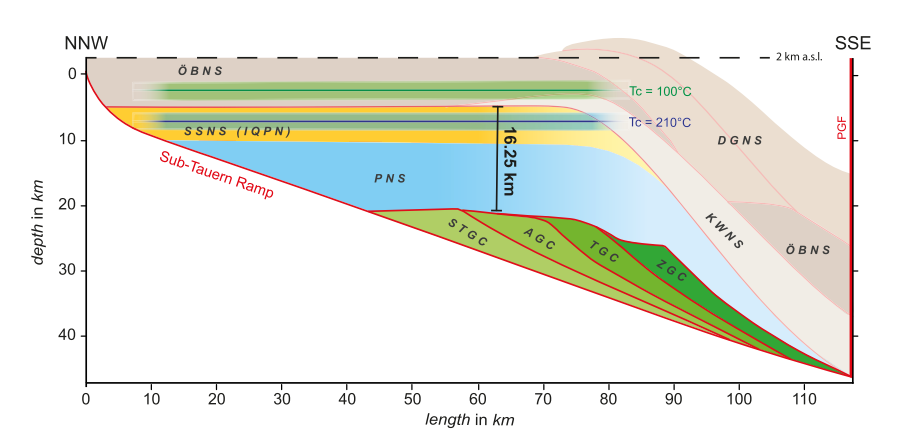


Figure 7. Reconstructed Penninic nappe system and Upper Austroalpine nappe system above the restored Venediger duplex of scenario 2 (Figure 6b). The northern limb of the Penninic nappe system and the Innsbrucker Quartzphyllite nappe could be quantitatively constrained by apatite fission-track (AFT) and zircon fission-track (ZFT) data sets (compilation of Bertrand et al., 2017), as only the former system was reset in the Miocene; partial annealing zone of AFT drawn in green and partial annealing zone of ZFT drawn in blue. The boundary between the Innsbrucker Quartzphyllite nappe and the Penninic nappe system was chosen by conserving the present-day nappe thickness ratio. The remaining nappes (light colors) were reconstructed qualitativley based on the situation to the west and southwest of the Brenner normal fault (Pomella et al., 2016). Abbreviations: AGC, Ahorn gneiss core; DGNS, Drauzug Gurktal nappe system; IQPN, Innsbrucker Quartzphyllite nappe; KWNS, Koralpe Wölz nappe system; ÖBNS, Ötztal Bundschuh nappe system; PGF, Pusteral Gailtal fault; SSNS, Silvretta Seckau nappe system; STGC, Subtauern gneiss core; TGC, Tuxer gneiss core; ZGC, Zillertaler gneiss core. Note: We have named only the Austroalpine nappe systems in this figure, not the nappes that belong to these systems. For nappe differentiation, we refer to Section 2.1.3 and Figures 1b and 1c.

Blanckenburg et al. (1989) (21 km). If we also take Fügenschuh et al. (1997) into account (23 km pre-indenter depth), the thicknesses stated above are increased by another 2 km, which would mean 19.3 km (deepest limit of AFT partial annealing zone) and 15.4 km (deepest limit of ZFT annealing zone) pre-indenter thickness, respectively. Hence, our modeling suggest the total pre-indenter thickness of the northern hanging-wall limbs (Innsbrucker Quartzphyllite and Penninic nappe system) was between 13.4 and 19.3 km, which is between ca. 25% and 48% more than today.

# 5. Discussion

### 5.1. Uncertainties of the Model

The accuracy of our restoration process depends on the constraints that we chose beforehand. Each constraint introduces a certain error into the model, which propagates throughout each step of the restoration. The uncertainties associated with the chosen constraints can be categorized as follows: (a) Errors from input data, (b) Errors related to keeping parameters constant over time, and (c) Errors arising from fundamental assumptions. We outline these errors in the following before discussing our results:

# • Errors from input data:

We used FT data of Most (2003) and from the compilation of Bertrand et al. (2017). Each cooling age has a certain error, which is on average  $\pm 0.71$  Ma  $\sigma 1$  for the samples taken for the restoration of the VD (Most, 2003; Supporting Information S1). The ZFT samples used for the modeling are located some 25 km east of the profile (see Figure 1b) and are projected onto the cross-section plane along the strike of the fold axes of the gneiss cores. In contrast to the samples used by Fügenschuh et al. (1997) and Wolff et al. (2020), they are therefore not located in the immediate area that is influenced by the BNF. Our thermal model is thus more orientated toward the work of Eizenhöfer et al. (2023), focusing on the TRANSALP corridor. An additional cooling effect of the BNF was therefore not taken into account. Fast tectonic unroofing by the BNF would shift the position of the ZFT annealing zone and the brittle to viscous transition upwards. In addition, the western TW plunges in a westerly direction due to the dragging along the BNF. We projected the ZFT data horizontally into the cross-section plane in order to keep their relative position to the surface unchanged, resulting in a position slightly above the VD (max. 3 km above the AGC). This generates an estimated temporal shift of ca. 1–2 Ma.

The temperature-time- and temperature-depth paths of von Blanckenburg et al. (1989) and Fügenschuh

RUDMANN ET AL. 14 of 22



et al. (1997) are based on data that contain errors (Figure 3). The error of each data point is indicated by a parallelogram (von Blanckenburg et al., 1989) or error bars (Fügenschuh et al., 1997). To get more information about their error calculation and the data on which their models are based, we refer to their publications. The deep structure of the cross-section (Reiter et al., 2018) is not well constraint and in part speculative.

• Errors related to keeping parameters constant over time:

We kept the shape of the present-day isotherms, the dip of the Sub-Tauern ramp, and the elevation constant. Varying shapes of the isotherms would change the amount of displacement required along the Sup-Tauern ramp, because these are dependent on the location in depth of the ZFT annealing zone.

A variation of the inclination of the Sub-Tauern ramp would influence the depth and horizontal shortening values during the restoration significantly.

Increasing the elevation (e.g., by erosion) would shift the partial annealing zones of ZFT and AFT, the brittle to viscous transition and the pre-indenter depth upwards, going backwards in time.

Errors arising from fundamental assumptions:

We assume the brittle-viscous transition at ca. 270–310°C, which is true for quartz using a characteristic natural strain rate and stress state (cf., Speckbacher et al., 2011; Stipp et al., 2002a). 10%–20% of a weak mineral phase, e.g., quartz and mica, is sufficient to weaken the rock rheologically by forming an interconnected weak layering (e.g., Handy, 1994). If not only dislocation creep but also other deformation mechanisms of polymineralic rock flow are active (e.g., Evans, 1988; Kilian et al., 2011; Mitra, 1984; O'Hara, 2007; Stünitz and Gerald, 1993; White, 2001; Wintsch et al., 1995), the brittle-viscous transition tend to shift to a lower temperature. However, more precise estimates on that condition cannot be made as the transition temperature depends on a number of further parameters (e.g., mineral content and proportion, grain size, grain distribution, fluid content). Therefore, the displacement of the entire VD below the 300° isotherm (Fügenschuh et al., 1997) represents a conservative estimate for the viscous to brittle transition, but the actual temperature is presumably lower and hence closer to the partial annealing zone of ZFT.

The closure temperature of fission-tracks depends on the cooling rate (Bernet & Garver, 2005). The brittle to viscous transition temperature depends on the strain rate (e.g., Stipp et al., 2002a). Both can change over time, which can increase or decrease the temperature difference between the two limits. This in turn affects (a) the temporal shift between the end of viscous folding and ZFT ages and (b) the offset of the VD below these boundaries.

Analogue models of Rosenberg et al. (2004, 2007) show that the indenter could also have been transported to the northeast, or at least a clockwise rotation could have occurred during indentation (Bertrand et al., 2017). This would reduce the north-directed transport to 60 km (see discussion by Rosenberg et al., 2018). Our model would then end beyond the loose pin. This could mean that (a) the deep structure of our cross-section is not correct, that (b) the 60 km is not correct, or that (c) reality lies somewhere in between.

We assume a symmetrical duplex as pre-indenter structure. A symmetrical duplex results from up-ramping of the "even" footwall (e.g., Boyer & Elliott, 1982). However, initial structures, such as a horst-graben system and maybe other tectonic features, may have been present prior to duplex formation in the orogenic wedge, which is why the pre-indenter duplex might not have been perfectly symmetrical.

We are aware that the input data brings errors into the model, that the most parameters were most likely not constant over time and that also some basic assumptions contain errors. However, the more constraints placed on a model, the more precise it becomes, despite the errors of the individual constraints. Our model gives minimum and maximum values, rather than exact values, but it provides a well-constrained approximation of the realistic deformation history of the western TW during the indenter stage. Nevertheless, we would like to clearly note that our model represents one possible Miocene deformation history and pre-indenter structure.

# 5.2. Miocene Deformation of the Western TW

At the beginning of indentation in the Early Miocene (e.g., Pomella et al., 2012; Schmid et al., 2013 and references therein; Verwater et al., 2021 and references therein), the top of the VD was situated at a depth of 21–23 km. These values result from the calculated temperature-time- and temperature-depth-paths of von Blanckenburg et al. (1989) and Fügenschuh et al. (1997), respectively, and an assumed topographic elevation of 2 km a.s.l. Our model suggests that the VD might have been a flat-lying, symmetrical duplex structure at that time (Figures 6 and 7). Subsequently, the first phase of incremental crustal shortening that occurred north of the approaching Dolomites indenter was

RUDMANN ET AL. 15 of 22

accommodated by upright folding of the VD. Our restoration yields two scenarios: in scenario 1 (Figure 6a), a duplex with an initial interlimb angle of ca. 160° of each horse, or gneiss core, respectively, became upright folded. Thereby, each gneiss core was folded by a different percentage, which increases from structural lowest to highest (STGC: 70%, AGC: 75%, TGC: 80%, ZGC: 85%). In contrast, in scenario 2 (Figure 6b), the VD compensated the crustal shortening by upright folding and coeval slip along the Sub-Tauern ramp. Here, the horses of the initial duplex structure had interlimb angles of 150°. Therefore, the amount of upright folding of the individual gneiss cores was less than in scenario 1 (STGC: 60%, AGC: 65%, TGC: 70%, TGC: 75%) to obtain the present-day structure of the VD. In this case, the synchronous offset along the Sub-Tauern ramp must have been minimum of 16 km until the crest of the TGC (highest-protruding gneiss core) reached the pre-indenter depth (Fügenschuh et al., 1997; von Blanckenburg et al., 1989). In both scenarios, the amount of folding of the gneiss cores increases toward the south, most likely because this was the site of the gneiss cores being in direct contact with the indenter.

Folding lasted as long as the felsic rocks of the VD were located in the viscous regime, that is above approximately 300°C. We modeled vertical extension of ca. 17 km in both scenarios, which is the distance between the upper limit of the pre-indenter depth in which the top of the VD was located (21 km b.s.l.; von Blanckenburg et al., 1989; Figure 6) and the position of the 300°C isotherm (ca. 4 km b.s.l. with a geothermal gradient of 50°C/km; Fügenschuh et al., 1997), assuming a constant elevation of 2 km a.s.l. This is quite similar to results of Fügenschuh et al. (1997) and Lammerer et al. (2008). However, they differ in timing. While Fügenschuh et al. (1997) calculated 15 km of exhumation until ca. 13 Ma and thermal conditions of the brittle to viscous transition at ca. 14 Ma (Figures 3a), Lammerer et al. (2008) postulate 13 km of increasing duplex height between 30 and 20 Ma. To approximate the time of the end of viscous folding, we use ZFT data. A cooling rate of 10°C/Ma prevailed between the latest onset of indentation (21 Ma) and the oldest ZFT cooling age (17  $\pm$  0.6 Ma; Fügenschuh et al., 1997; Figure 3a), this means cooling below 235°C ± 30°C (Brandon et al., 1998; Reiners & Brandon, 2006). The timing of the brittle-viscous transition at approximately 300°C for each gneiss core thus shifts to a slightly earlier age than that of the respective ZFT data. This timeshift is at least 0.5-3.5 Ma, which results from the difference between the lower limit of the partial annealing zone of ZFT (265°C; Brandon et al., 1998; Reiners & Brandon, 2006) and the brittle-viscous transition range (270-310°C; cf. van Daalen et al., 1999; Stöckhert et al., 1999; Stipp et al., 2002b). Between 17 and 9 Ma, the cooling rate increased to  $50^{\circ}$ C/Ma (Fügenschuh et al., 1997; Figure 3a), which shifted the partial annealing zone of ZFT to  $250 \pm 30^{\circ}$ C (Brandon et al., 1998; Reiners & Brandon, 2006) and thus overlapped with the brittle-viscous transition range. The aforementioned timeshift is negligible in this case.

In any case, we think that upright folding did not stop abruptly, but might have carried on during the Early and Middle Miocene. During this time span, the folds became more and more locked at the top of the VD, as they entered the brittle regime, while viscous deformation continued at the root of the duplex by the progressive wedging of the Dolomites indenter. This probably caused the south-vergence of the entire western TW and e.g., the verticalization and locally even overturning of the westernmost Pustertal Gailtal fault segment of the Periadriatic fault system. In general, the south-vergence and the upright folding is strongest in the westernmost TW, where the Dolomites indenter indents the most northwards (e.g., Klotz et al., 2019; Rosenberg et al., 2015; Schmid et al., 2004, 2013). This implies that the Alpine viscous deformation, which created the individual structures of the Subpenninic domes across the TW, is directly linked to the amount of indentation of the eastern Southern Alps, and is therefore of Late Oligocene to Miocene age.

If we had used line-length balancing, as done by Schmid et al. (2013) and Rosenberg and Berger (2009), the surface area would have decreased during restoration, which would mean that material left the plane of cross-section back in time. This was presumably not the case in the western TW, but the opposite. W-E extension would have to transport material back into the plane backwards in time, which would mean that the area would have to increase. However, with our restoration of the VD, we extended the model ca. 70 km to the south by conserving the surface area as a minimum criterion, thus equaling shortening in front of the indenter (Figures 2, 6 and 7). We therefore conclude that no important amounts of material left the plane of cross-section by orogen-parallel extension in the westernmost TW. However, the situation for the northern limbs of the hanging-wall nappes (i.e., the Innsbrucker Quartzphyllite nappe and the northern part of the Penninic nappe system) is different. Surface samples from the Innsbrucker Quartzphyllite nappe reveal that they must have reached thermal conditions between the partial annealing zones of AFT and ZFT (Figure 1b; which is between 130 and 180°C, respectively, assuming a cooling rate of 1°C/Ma; Brandon et al., 1998; Reiners & Brandon, 2006; see also Figure 3) as only the former system was reset in the Mid-Miocene (Figure 1b). Assuming a pre-indenter geothermal gradient of 23°C/km (mean value of

RUDMANN ET AL. 16 of 22

von Blanckenburg et al. (1989) and Fügenschuh et al. (1997); Figures 3a and 3b), we found that the total thickness of the Innsbrucker Quartzphyllite nappe and the Penninic nappe system together is ca. 38% more after restoration (ca. 16.25 km; Figure 7) compared to the present-day total thickness of ca. 10 km (Figure 2a). This is, when the top of the Innsbrucker Quatzphyllite is placed half-way between the deepest limit of the partial annealing zone of AFT (130°C and 3.7 km b.s.l., respectively) and the upper limit of the partial annealing zone of ZFT (180°C and 5.8 km b.s.l., respectively), i.e. at 4.75 km. However, it could also have been possible that the top of the Innsbrucker Quartzphyllite was directly located at the deepest limit of the partial annealing zone of AFT, or directly at the deepest limit of the partial annealing zone of ZFT. Taking into account the pre-indenter depths of von Blanckenburg et al. (1989) and Fügenschuh et al. (1997), this result in a total pre-indenter thickness range of 13.4–19.3 km, which means a thickness reduction of ca. 25%–48%, with respect to the present-day. We postulate that the extension on the BNF was most likely responsible for this tectonic thinning. Lateral extrusion played most probably only a minor role in the westernmost TW, because the offsets of the strike-slip faults and shear zones that were involved in the lateral extrusion process are assumed to decay to zero displacement in the western TW—at least the shear zones within the VD (e.g., Rosenberg & Schneider, 2008; Scharf et al., 2013; Töchterle et al., 2011).

According to Schneider et al. (2013), the activity of the steep sinistral shear zones that dissect the western TW ranges from  $33.8 \pm 1$  to  $15.77 \pm 5.8$  Ma (Ahorn shear zone), over  $24.27 \pm 1.8$  Ma to  $12.47 \pm 1.0$  Ma (Tuxer shear zones) to  $20.37 \pm 2.0$  Ma to  $7.37 \pm 2.7$  Ma (Greiner shear zone). The latter's activity was dated by Pollington and Baxter (2010, 2011) to 28-20 Ma. This implies that they were already active before the Miocene indentation (e.g., Favaro et al., 2017; Pomella et al., 2011, 2012; Scharf et al., 2013; Schmid et al., 2013). We therefore assume that these shear zones did not originate during the Miocene indentation process, but might have been older, steep structures that had already traversed the flat VD beforehand and were reactivated during Miocene indentation.

When folding of the top of the VD finally terminated, ongoing crustal shortening north of the Dolomites indenter resulted in ca. 21 km offset of the entire VD along the Sub-Tauern ramp to its present-day position (Figure 5). This correlates with 20 km horizontal shortening and 7.3 km vertical uplift. This is similar to results of the kinematic model of Lammerer et al. (2008). They reconstructed 17 km of displacement along the Sub-Tauern ramp and 8 km uplift, starting after upright folding ca. 20 Ma ago. However, Lammerer et al. (2008) modeled a scenario, in which the deepest gneiss core (STGC) was formed after upright folding by progressive ramp propagation toward the north. In our restoration, we did not restore the STGC by down-ramping before unfolding, as not enough information about the deep structure of our model exists. We kept it as simple as possible (i.e., following Occam's Razor), but cannot rule out the more complex ramp model of Lammerer et al. (2008). Nevertheless, our results appear to be quite consistent with those of Lammerer et al. (2008).

Between 15 and 12 Ma, the main phase of back-thrusting along WSW-ENE-striking faults in the Dolomites indenter began (e.g., Valsugana fault system; see e.g., compilation in Eizenhöfer et al., 2023; Sieberer et al., 2023; Verwater et al., 2021). We hypothesize that there might be a causal relationship, whereby crustal shortening initially manifested through upright folding subsequently transitioned into both northward displacement of the VD along the Sub-Tauern ramp and back-thrusting in the eastern Southern Alps (see also McPhee & Handy, 2024).

In summary, our model evinces that the crustal shortening north of the indenter front was compensated by the VD in two different ways: in the first phase, by upright folding and, in the second phase, by northward displacement of the entire duplex along the Sub-Tauern ramp. In scenario 1, horizontal shortening amounts to ca. 50 km by upright folding and ca. 20 km by displacement along the Sub-Tauern ramp. Scenario 2 provides ca. 35 km of horizontal shortening by upright folding and ca. 35 km by displacement. Both scenarios reveal 17 km of vertical extension and 7.3 km (scenario 1) or 9.3 km (scenario 2) of vertical uplift by displacement along the Sub-Tauern ramp. The latter values correlate with the model of Eizenhöfer et al. (2023), who postulate ca. 10 km of exhumation of the western TW, as the result of displacement along the Sub-Tauern ramp.

# 6. Summary and Conclusions

Based on our kinematic restoration, the deformation history of the western TW during indentation can be summarized as follows:

• Crustal shortening north of the Dolomites indenter front was accommodated in the first phase by upright folding of the VD and in the second phase by northward displacement of the entire VD along the Sub-Tauern

RUDMANN ET AL. 17 of 22

- ramp. Two scenarios could be realistic during the folding phase: Only upright folding (scenario 1) or upright folding with coeval displacement along the Sub-Tauern ramp (scenario 2).
- In the first phase, folding leads to ca. 50 km (scenario 1) or ca. 35 km (scenario 2) of horizontal shortening.
   Displacement of the entire VD along the Sub-Tauern ramp resulted in ca. 20 km (scenario 1) or ca. 35 km
   (scenario 2) horizontal transport. In both scenarios, the VD was extended vertically by 17 km, while
   displacement along the Sub-Tauern ramp produced 7.3 km (scenario 1) or 9.3 km (scenario 2) vertical uplift.
- Folding started to cease slightly earlier than  $17 \pm 0.6$  Ma at the top of the ZGC. At that time, a geothermal gradient of  $50^{\circ}$ C/km prevailed. Folding locked at the top of the gneiss cores of the VD as they entered further into the brittle regime. Viscous deformation continued at the root of the VD through progressive wedging of the Dolomites indenter. This leads to a slightly south-vergence of the entire western TW.
- During upright folding, no significant amount of material of the VD was transported laterally out of the cross-section plane. In contrast, the Innsbrucker Quartzphyllite nappe and the northern part of the Penninic nappe system on top of the VD experienced significant tectonic thinning, which corresponds to a 25%–48% reduction of the total nappe-stack thickness. We think that the BNF most likely caused this tectonic thinning and lateral extrusion was barely involved.
- The southward extension of our model after retro-deformation, that is, the entire horizontal transport of the VD, amounts to ca. 70 km, which fits well to the amount of sinistral strike-slip movement along the Giudicarie fault system (ca. 75 km), indicating N to NNW-directed indentation.

# **Data Availability Statement**

The simplified tectonic map of the research area is based on AA.VV. (1930a, 1930b, 1960a, 1960b), Amt für Geologie und Baustoffprüfung (2007), Autonome Provinz Bozen-Südtirol (2014), Geosphere Austria (2017), Kreuss (2013, 2018), Moser (2011, 2012), Moser and Pavlik (2014), Rockenschaub and Nowotny (2009), Rockenschaub et al. (2011), Schmid et al. (2013), and Töchterle et al. (2007). For the cross-section, we used information of Brandner et al. (2008b), Reiter et al. (2018), Rosenberg & Garcia (2011), Schmid et al. (2013), and Töchterle et al. (2007). Thermochronological data were taken from Most (2003) and the compilation of Bertrand et al. (2017). The present-day isotherms were taken from Eizenhöfer et al. (2023). We used temperature-time and temperature-depth paths of Fügenschuh et al. (1997) and von Blanckenburg et al. (1989). Digital elevation models (25 m resolution) used for the topographic profile are available through European Environmental European Environment Agency (2016).

# Acknowledgments

We would like to thank the Editor, Prof. Dr. Diordie Grujic, and reviews by Sebastian Oriolo and one anonymous reviewer. Both reviewers contributed to a significant improvement of the manuscript with their very constructive and helpful comments. We thank Mark Handy, Stefan Schmid, Paul Eizenhöfer, Peter McPhee, Rüdiger Kilian, Rebecca Kühn, Simon Hinterwirth, Anna-Katharina Sieberer, Thomas Klotz, Hugo Ortner, and the entire AlpArray community for the very enriching discussions. We gratefully acknowledge funding from the German Science Foundation (TA 427/5-1, BR 3779/6-1, STI 298/11-1) within the Priority Programme SSP-2017 "Mountain **Building Processes in Four Dimensions** (MB-4D)." We thank Petroleum Experts Ltd. for the use of an Academic Licence of MOVETM. Open Access funding enabled and organized by Projekt DEAL.

# References

AA.VV. (1930a). Carta Geologica della Tre Venezie, Foglio 1<sup>A</sup>. Vetta d'Italia. Servizio Geologico d'Italia (Map).

AA.VV. (1930b). Carta Geologica della Tre Venezie, Foglio 4<sup>A</sup>, Bressanone. Servizio Geologico d'Italia (Map).

AA.VV. (1960a). Carta Geologica d'Italia, Foglio 4, Merano. Servizio Geologico d'Italia (Map).

AA.VV. (1960b). Carta Geologica d'Italia, Foglio 4<sup>A</sup>, Bressanone. Servizio Geologico d'Italia (Map).

Amt für Geologie und Baustoffprüfung. (2007). Geologische Übersicht von Südtirol und der angrenzenden Gebiete (Geologische Haupteinheiten, Hauptstörungen) (Map). Retrieved from http://geokatalog.buergernetz.bz.it/geokatalog/#!

Autonome Provinz Bozen-Südtirol. (2014). Geobrowser maps (map). Retrieved from https://maps.civis.bz.it/

Axen, G. J., Bartley, J. M., & Selverstone, J. (1995). Structural expression of a rolling hinge in the footwall of the Brenner Line normal fault, eastern Alps. *Tectonics*, 14(6), 1380–1392. https://doi.org/10.1029/95tc02406

Ballian, A., Meijers, M. M. J., Cojan, I., Huygue, D., Methner, K., Boateng, D., et al. (2024). Stable isotope paleoaltimetry reveals Early to Middle Miocene along-strike elevation differences of the European Alps. EGU General Assembly, 2024, EGU24-18901. https://doi.org/10.5194/egusphere-egu24-18901

Balling, P., Tomljenović, B., Schmid, S. M., & Ustaszewski, K. (2021). Contrasting along-strike deformation styles in the central external Dinarides assessed by balanced cross-sections: Implications for the tectonic evolution of its Paleogene flexural foreland basin system. *Global and Planetary Change*, 205, 103587. https://doi.org/10.1016/j.gloplacha.2021.103587

Barnes, J. D., Selverstone, J., & Sharp, Z. D. (2004). Interactions between serpentinite devolatilization, metasomatism and strike-slip strain localization during deep-crustal shearing in the Eastern Alps. *Journal of Metamorphic Geology*, 22(4), 283–300. https://doi.org/10.1111/j. 1525-1314.2004.00514.x

Behrmann, J. H. (1988). Crustal-scale extension in a convergent orogen: The Sterzing-Steinach mylonite zone in the eastern Alps. *Geodinamica Acta*, 2(2), 63–73. https://doi.org/10.1080/09853111.1988.11105157

Behrmann, J. H., & Frisch, W. (1990). Sinistral ductile shearing associated with metamorphic decompression in the Tauern Window, Eastern Alps. *Jahrbuch der Geologischen Bundesanstalt*, 133(2), 135–146.

Berger, A., Rosenberg, C. L., & Molli, G. (2024). Cenozoic magmatism in the Alps and their surroundings: Relating magmatic and geodynamic events. In C. L. Rosenberg & N. Bellahsen (Eds.), *Geodynamics of the Alps 3: Collisional processes* (Vol. 3, pp. 1–52). https://doi.org/10.1002/9781394299560.ch1

Bernet, M., & Garver, J. I. (2005). Fission-track analysis of detrital zircon. Reviews in Mineralogy and Geochemistry, 58(1), 205–237. https://doi.org/10.2138/rmg.2005.58.8

RUDMANN ET AL. 18 of 22

2025, 7, Downloadec

1029/2024TC008371 by Martin

- Berryman, E. J., Kutzschbach, M., Trumbull, R. B., Meixner, A., van Hinsberg, V., Kasemann, S. A., & Franz, G. (2017). Tourmaline as a petrogenetic indicator in the Pfitsch Formation, western Tauern window, eastern Alps. *Lithos*, 284, 138–155. https://doi.org/10.1016/j.lithos. 2017.04.008
- Bertrand, A., Rosenberg, C., Rabaute, A., Herman, F., & Fügenschuh, B. (2017). Exhumation mechanisms of the Tauern Window (Eastern Alps) inferred from apatite and zircon fission track thermochronology [Dataset]. *Tectonics*, 36(2), 207–228. https://doi.org/10.1002/2016tc004133
- Bistacchi, A., Massironi, M., & Menegon, L. (2010). Three-dimensional characterization of a crustal-scale fault zone: The Pusteria and Sprechenstein fault system (Eastern Alps). *Journal of Structural Geology*, 32(12), 2022–2041. https://doi.org/10.1016/j.jsg.2010.06.003
- Borsi, S., Del Moro, A., Sassi, F. P., & Zirpoli, G. (1973). Metamorphic evolution of the Austridic rocks to the south of the Tauern window (eastern Alps): Radiometric and geopetrological data. *Memorie della Societa Geologica Italiana*, 12, 549–571.
- Boyer, S. E., & Elliott, D. (1982). Thrust systems. AAPG Bulletin, 66(9), 1196–1230. https://doi.org/10.1306/03B5A77D-16D1-11D7-8645000102C1865D
- Brandes, C., Schmidt, C., Tanner, D. C., & Winsemann, J. (2013). Paleostress pattern and salt tectonics within a developing foreland basin (north-western Subhercynian Basin, northern Germany). *International Journal of Earth Sciences*, 102(8), 2239–2254. https://doi.org/10.1007/s00531-013-0911-7
- Brandes, C., Tanner, D. C., & Winsemann, J. (2016). Kinematic 3-D retro-modeling of an orogenic bend in the South Limón fold-and-thrust belt, eastern Costa Rica: Prediction of the incremental internal strain distribution. *Pure and Applied Geophysics*, 173(10–11), 3341–3356. https://doi.org/10.1007/s00024-016-1263-6
- Brandner, R. (2013). Alpenprofil. Institute for Geology. University of Innsbruck. https://doi.org/10.13140/RG.2.2.20466.81603
- Brandner, R., Reiter, F., & Töchterle, A. (2008a). Hochmetamorphe Keuperfazies ("Aigerbach-Formation") und unterjurassische Kontinentalrandfazies ("Kaserer-Formation"), zwei Schlüssellithologien bei der geologischen Prognose für den Brenner-Basistunnel. *Journal of Alpine Geology*, 49, 14. https://doi.org/10.13140/RG.2.2.33416.21763
- Brandner, R., Reiter, F., & Töchterle, A. (2008b). Überblick zu den Ergebnissen der geologischen Vorerkundung für den Brenner-Basistunnel [Cross-section]. *Geologie Alpine*, 5, 165–174.
- Brandon, M. T., Roden-Tice, M. K., & Garver, J. I. (1998). Late Cenozoic exhumation of the Cascadia accretionary wedge in the Olympic Mountains, northwest Washington state. *Geological Society of America Bulletin*, 110(8), 985–1009. https://doi.org/10.1130/0016-7606(1998) 110%3C0985;LCEOTC%3E2.3.CO:2
- Coward, M. P. (1996). Balancing sections through inverted basins. Geological Society, London, Special Publications, 99(1), 51–77. https://doi.org/10.1144/GSL.SP.1996.099.01.06
- Dahlstrom, C. D. A. (1969). Balanced cross sections. Canadian Journal of Earth Sciences, 6(4), 743–757. https://doi.org/10.1139/e69-069 De Paor, D. G. (1988). Balanced section in thrust belts part 1: Construction. AAPG Bulletin, 72(1), 73–90. https://doi.org/10.1306/703c81cd-1707-11d7-8645000102c1865d
- Eizenhöfer, P. R., Glotzbach, C., Büttner, L., Kley, J., & Ehlers, T. A. (2021). Turning the orogenic switch: Slab-reversal in the Eastern Alps recorded by low-temperature thermochronology. *Geophysical Research Letters*, 48(6), e2020GL092121. https://doi.org/10.1029/2020GL092121
- Eizenhöfer, P. R., Glotzbach, C., Kley, J., & Ehlers, T. A. (2023). Thermo-kinematic evolution of the Eastern European Alps along the TRANSALP transect [Dataset]. *Tectonics*. https://doi.org/10.1029/2022TC007380
- European Environment Agency. (2016). EU-DEM (raster)—Version 1.1, Apr. 2016 [Dataset]. Retrieved from https://sdi.eea.europa.eu/catalogue/srv/api/records/3473589f-0854-4601-919e-2e7dd172ff50
- Evans, J. P. (1988). Deformation mechanisms in granitic rocks at shallow crustal levels. *Journal of Structural Geology*, 10(5), 437–443. https://doi.org/10.1016/0191-8141(88)90031-4
- Favaro, S., Handy, M. R., Scharf, A., & Schuster, R. (2017). Changing patterns of exhumation and denudation in front of an advancing crustal indenter, Tauern Window (Eastern Alps). *Tectonics*, 36(6), 1053–1071. https://doi.org/10.1002/2016TC004448
- Frasl, G. (1958). Zur Seriengliederung der Schieferhülle in den mittleren Hohen Tauern. Jahrbuch der Geologischen Bundesanstalt, 101, 323-472.
- Frasl, G., & Frank, W. (1966). Einführung in die Geologie und Petrographie des Penninikums im Tauernfenster mit besonderer Berücksichtigung des Mittelabschnittes im Oberpinzgau, Land Salzburg. Der Aufschluss, Sonderheft, 15, 30–58.
- Frisch, W. (1974). Die stratigraphisch-tektonische Gliederung der Schieferhülle und die Entwicklung des penninischen Raumes im westlichen Tauernfenster (Gebiet Brenner-Gerlospaß). Mitteilungen der Geologischen Gesellschaft in Wien, 66(67), 9–20.
- Frisch, W. (1977). Der alpidische Internbau der Venedigerdecke im westlichen Tauernfenster. Neues Jahrbuch Geologische und Paläontologische Monatshefte, 11, 675–696.
- Frisch, W. (1979). Tectonic progradation and plate tectonic evolution of the Alps. *Tectonophysics*, 60(3–4), 121–139. https://doi.org/10.1016/0040-1951(79)90155-0
- Frisch, W. (1980). Post-hercynian formations of the western Tauern window: Sedimentological features, depositional environment, and age. *Mitteilungen der Osterreichischen Geologischen Gesellschaft*, 71(72), 49–63.
- Frisch, W., Dunkl, I., & Kuhlemann, J. (2000). Post-collisional orogen-parallel large-scale extension in the Eastern Alps. *Tectonophysics*, 327(3–4), 239–265. https://doi.org/10.1016/S0040-1951(00)00204-3
- Frisch, W., Kuhlemann, J., Dunkl, I., & Brügel, A. (1998). Palinspastic reconstruction and topographic evolution of the Eastern Alps during late Tertiary tectonic extrusion. *Tectonophysics*, 297(1–4), 1–15. https://doi.org/10.1016/S0040-1951(98)00160-7
- Froitzheim, N., Schmid, S., & Conti, P. (1994). Repeated change from crustal shortening to orogen-parallel extension in the Austroalpine units of Graub unden. *Eclogae Geologicae Helvetiae*, 87(2), 559–612.
- Fügenschuh, B., Mancktelow, N. S., & Schmid, S. M. (2012). Comment on Rosenberg and Garcia: Estimating displacement along the Brenner fault and orogen-parallel extension in the eastern Alps. *International Journal of Earth Sciences*, 101(5), 1451–1455. https://doi.org/10.1007/s00531-011-0725-4
- Fügenschuh, B., Seward, D., & Mancktelow, N. (1997). Exhumation in a convergent orogen: The western Tauern window [Dataset]. *Terra Nova*, 9(5-6), 213–217. https://doi.org/10.1046/j.1365-3121.1997.d01-33.x
- Genser, J., & Neubauer, F. (1989). Low angle normal faults at the eastern margin of the Tauern window (Eastern Alps). Mitteilungen der Osterreichischen Geologischen Gesellschaft, 81, 233–243.
- Geosphere Austria. (2017). Multithematische geologische Karte von Österreich 1:1.000.000 (Map). Retrieved from https://www.arcgis.com/apps/mapviewer/index.html?webmap=b922bcd335d645e091f53aa79782a8d9
- Groß, P., Handy, M. R., John, T., Pestal, G., & Pleuger, J. (2020). Crustal-scale sheath folding at HP conditions in an exhumed Alpine subduction zone (Tauern Window, Eastern Alps). Tectonics, 39(2), e2019TC005942. https://doi.org/10.1029/2019TC005942

RUDMANN ET AL. 19 of 22

2025, 7, Downle

- Groß, P., Pleuger, J., & Handy, M. R. (2022). Rift-Related paleogeography of the European margin in the eastern Alps (central Tauern window). Swiss Journal of Geosciences, 115(1), 1–40. https://doi.org/10.1186/s00015-022-00426-9
- Groß, P., Pleuger, J., Handy, M. R., Germer, M., & John, T. (2021). Evolving temperature field in a fossil subduction channel during the transition from subduction to collision (Tauern Window, Eastern Alps). *Journal of Metamorphic Geology*, 39(2), 247–269. https://doi.org/10.1111/jmg. 12572
- Handy, M. R. (1994). Flow laws for rocks containing two non-linear viscous phases: A phenomenological approach. *Journal of Structural Geology*, 16(3), 287–301. https://doi.org/10.1016/0191-8141(94)90035-3
- Handy, M. R., Schmid, S. M., Bousquet, R., Kissling, E., & Bernoulli, D. (2010). Reconciling plate-tectonic reconstructions of Alpine Tethys with the geological–geophysical record of spreading and subduction in the Alps. Earth-Science Reviews, 102(3–4), 121–158. https://doi.org/10. 1016/j.earscirev.2010.06.002
- Höck, V., & Koller, F. (1989). Magmatic evolution of the Mesozoic ophiolites in Austria. Chemical Geology, 77(3-4), 209-227. https://doi.org/10.1016/0009-2541(89)90075-2
- Jourdon, A., Rolland, Y., Petit, C., & Bellahsen, N. (2014). Style of Alpine tectonic deformation in the Castellane fold-and-thrust belt (SW Alps, France): Insights from balanced cross-sections. *Tectonophysics*, 633, 143–155. https://doi.org/10.1016/j.tecto.2014.06.022
- Kilian, R., Heilbronner, R., & Stünitz, H. (2011). Quartz grain size reduction in a granitoid rock and the transition from dislocation to diffusion creep. Journal of Structural Geology, 33(8), 1265–1284. https://doi.org/10.1016/j.jsg.2011.05.004
- Klotz, T., Pomella, H., Reiser, M., Fügenschuh, B., & Zattin, M. (2019). Differential uplift on the boundary between the eastern and the southern European Alps: Thermochronologic constraints from the Brenner base tunnel. *Terra Nova*, 31(3), 281–294. https://doi.org/10.1111/ter.12398
- Koller, F., & Prestal, G. (2003). Die ligurischen Ophiolite der Tarntaler Berge und der Matreier Zone. Arbeitstagung der Geologische Bundesanstalt. Blatt, 148, 65–76.
- Kreuss, O. (2013). Geologische Karte der Republik Österreich 1:50.000 GEOFAST (Blatt 176 Mühlbach) (Map). Geologische Bundesanstalt. Kreuss, O. (2018). Geologische Karte der Republik Österreich 1:50.000 GEOFAST (Blatt 149 Lanersbach) (Map). Geologische Bundesanstalt. Lammerer, B. (1986). Das Autochthon im westlichen Tauernfenster. Jahrbuch der Geologischen Bundesanstalt, 129, 51–67.
- Lammerer, B., Gebrande, H., Lüschen, E., & Veselá, P. (2008). A crustal-scale cross-section through the Tauern Window (eastern Alps) from geophysical and geological data. Geological Society, London, Special Publications, 298(1), 219–229. https://doi.org/10.1144/SP298.11
- Lammerer, B., & Weger, M. (1998). Footwall uplift in an orogenic wedge: The Tauern window in the eastern Alps of Europe. *Tectonophysics*, 285(3–4), 213–230. https://doi.org/10.1016/S0040-1951(97)00272-2
- Laubscher, H. P. (1971). Das Alpen-Dinariden-Problem und die Palinspastik der südlichen tethys. Geologische Rundschau, 60(3), 813–833. https://doi.org/10.1007/bf02046522
- Linzer, H. G., Decker, K., Peresson, H., Dell'Mour, R., & Frisch, W. (2002). Balancing lateral orogenic float of the Eastern Alps. *Tectonophysics*, 354(3–4), 211–237. https://doi.org/10.1016/S0040-1951(02)00337-2
- Luth, S. W., & Willingshofer, E. (2008). Mapping of the post-collisional cooling history of the Eastern Alps. Swiss Journal of Geosciences, 101(S1), 207–223. https://doi.org/10.1007/s00015-008-1294-9
- Mancktelow, N. S., Stöckli, D. F., Grollimund, B., Müller, W., Fügenschuh, B., Viola, G., et al. (2001). The DAV and Periadriatic fault systems in the Eastern Alps south of the Tauern window. *International Journal of Earth Sciences*, 90(3), 593–622. https://doi.org/10.1007/s005310000190
- Marshak, S., & Wilkerson, M. S. (2004). Fold-thrust belts. In Earth structure: An introduction to structural geology and tectonics (2nd ed., pp. 444–474). WW Norton & Company, Inc.
- Massironi, M., Bistacchi, A., & Menegon, L. (2011). Misoriented faults in exhumed metamorphic complexes: Rule or exception? Earth and Planetary Science Letters, 307(1–2), 233–239. https://doi.org/10.1016/j.epsl.2011.04.041
   McPhee, P. J., Altıner, D., & Van Hinsbergen, D. J. (2018). First balanced cross section across the Taurides fold-thrust belt: Geological constraints
- on the subduction history of the Antalya slab in southern Anatolia. *Tectonics*, 37(10), 3738–3759. https://doi.org/10.1029/2017TC004893 McPhee, P. J., & Handy, M. R. (2024). Post-collisional reorganisation of the Eastern Alps in 4D—Crust and mantle structure. *Tectonics*, 43(8), e2024TC008374. https://doi.org/10.1029/2024TC008374
- Mitra, G. (1984). Brittle to ductile transition due to large strains along the White Rock thrust, Wind River Mountains, Wyoming. *Journal of Structural Geology*, 6(1–2), 51–61. https://doi.org/10.1016/0191-8141(84)90083-x
- Moser, M. (2011). Geologische Karte der Republik Österreich 1:50.000—GEOFAST (Blatt 147 Axams) (Map). Geologische Bundesanstalt.
- Moser, M. (2012). Geologische Karte der Republik Österreich 1:50.000—GEOFAST (Blatt 174 Timmelsjoch) (Map). Geologische Bundesanstalt. Moser, M., & Pavlik, W. (2014). Geologische Karte der Republik Österreich 1:50.000—GEOFAST (Blatt 150 Mayrhofen) (Map). Geologische
- Most, P. (2003). Late Alpine cooling histories of tectonic blocks along the central part of the Transalp-Traverse (Inntal-Gadertal): Constraints from geochronology (PhD thesis) [Dataset]. *Univ. of Tübingen*. Retrieved from https://www.google.com/url?sa=t&source=web&rct=j&opi=89978449&url=https://publikationen.uni-tuebingen.de/xmlui/bitstream/10900/48447/1/pdf/DissPetraMost.pdf&ved=2ahUKEwihyZPN xaiOAxX5BdsEHWmPMBQQFnoECBkQAQ&usg=AOvVaw1i11KfhsoSFBIiAOYoIfpf
- Neubauer, F. (1994). Kontinentkollision in den Ostalpen. Geowissenschaften, 12, 136-140.
- Neubauer, F., Genser, J., & Handler, R. (2000). The eastern Alps: Result of a two-stage collision process. *Mitteilungen der Osterreichischen Geologischen Gesellschaft*, 92(1999), 117–134.
- O'Hara, K. (2007). Reaction weakening and emplacement of crystalline thrusts: Diffusion control on reaction rate and strain rate. *Journal of Structural Geology*, 29(8), 1301–1314. https://doi.org/10.1016/j.jsg.2007.04.004
- Ortner, H., Reiter, F., & Brandner, R. (2006). Kinematics of the Inntal shear zone–sub-Tauern ramp fault system and the interpretation of the TRANSALP seismic section, Eastern Alps, Austria. *Tectonophysics*, 414(1–4), 241–258. https://doi.org/10.1016/j.tecto.2005.10.017
- Pennacchioni, G., & Mancktelow, N. S. (2007). Nucleation and initial growth of a shear zone network within compositionally and structurally heterogeneous granitoids under amphibolite facies conditions. *Journal of Structural Geology*, 29(11), 1757–1780. https://doi.org/10.1016/j.jsg. 2007.06.002
- Pennacchioni, G., & Mancktelow, N. S. (2013). Initiation and growth of strike-slip faults within intact metagranitoid (Neves area, eastern Alps, Italy). *Bulletin*, 125(9–10), 1468–1483. https://doi.org/10.1130/B30832.1
- Pollington, A. D., & Baxter, E. F. (2010). HighresolutionSm–Nd garnet geochronology reveals the uneven pace of tectonometamorphic processes. Earth and Planetary Science Letters, 293(1–2), 63–71. https://doi.org/10.1016/j.epsl.2010.02.019
- Pollington, A. D., & Baxter, E. F. (2011). High precision microsampling and preparation of zoned garnetporphyroblasts for Sm-Nd geochronology. Chemical Geology, 281(3-4), 270-282. https://doi.org/10.1016/j.chemgeo.2010.12.014
- Pomella, H., Flöss, D., Speckbacher, R., Tropper, P., & Fügenschuh, B. (2016). The western end of the Eoalpine high-pressure belt (Texel unit, south Tyrol/Italy). *Terra Nova*, 28(1), 60–69. https://doi.org/10.1111/ter.12191

RUDMANN ET AL. 20 of 22

- Pomella, H., Klötzli, U., Scholger, R., Stipp, M., & Fügenschuh, B. (2011). The Northern Giudicarie and the Meran-Mauls fault (Alps, Northern Italy) in the light of new paleomagnetic and geochronological data from boudinaged Eo-/Oligocene tonalites. *International Journal of Earth Sciences*, 100(8), 1827–1850. https://doi.org/10.1007/s00531-010-0612-4
- Pomella, H., Stipp, M., & Fügenschuh, B. (2012). Thermochronological record of thrusting and strike-slip faulting along the Giudicarie fault system (Alps, Northern Italy). *Tectonophysics*, 579, 118–130. https://doi.org/10.1016/j.tecto.2012.04.015
- Ratschbacher, L., Frisch, W., Linzer, H. G., & Merle, O. (1991). Lateral extrusion in the eastern Alps, part 2: Structural analysis. *Tectonics*, 10(2), 257–271. https://doi.org/10.1029/90TC02623
- Ratschbacher, L., Merle, O., Davy, P., & Cobbold, P. (1991). Lateral extrusion in the eastern Alps, part 1: Boundary conditions and experiments scaled for gravity. *Tectonics*, 10(2), 245–256. https://doi.org/10.1029/90TC02622
- Reicherter, K., Fimmel, R., & Frisch, W. (1993). Sinistral strike-slip faults in the central Tauern window (Eastern Alps, Austria). Jahrbuch der Geologischen Bundesanstalt, 136, 495–502.
- Reiners, P. W., & Brandon, M. T. (2006). Using thermochronology to understand orogenic erosion. *Annual Review of Earth and Planetary Sciences*, 34(1), 419–466. https://doi.org/10.1146/annurev.earth.34.031405.125202
- Reiter, F., Freudenthaler, C., Hausmann, H., Ortner, H., Lenhardt, W., & Brandner, R. (2018). Active seismotectonic deformation in front of the Dolomites indenter, eastern Alps [Cross-section]. *Tectonics*, 37(12), 4625–4654. https://doi.org/10.1029/2017TC004867
- Reiter, F., Lenhardt, W. A., Decker, K., & Brandner, R. (2003). Aktive Tektonik und Seismizität im Bereich Wipptal-Inntal. Andauern der lateralen Extrusion? Arbeitstagung der Geologische Bundesanstalt. Blatt, 148, 179–184.
- Ricchi, E., Bergemann, C. A., Gnos, E., Berger, A., Rubatto, D., Whitehouse, M. J., & Walter, F. (2020). Cenozoic deformation in the Tauern Window (Eastern Alps) constrained by in situ Th-Pb dating of fissure monazite. *Solid Earth*, 11(2), 437–467. https://doi.org/10.5194/se-11-437-2020
- Rockenschaub, M., Kolenprat, B., & Nowotny, A. (2003). Das westliche Tauernfenster. Arbeitstagung der Geologische Bundesanstalt. Blatt, 148, 7–38
- Rockenschaub, M., & Nowotny, A. (2009). Geologische Karte der Republik Österreich 1:50.000 (Blatt 148 Brenner) (Map). Geologische Bundesanstalt
- Rockenschaub, M., Nowotny, A., Brandner, R., Fenti, V., Frisch, W., Friz, C., et al. (2011). Geologische Karte der Republik Österreich 1:50.000 (Blatt 175 Sterzing) (Map). Geologische Bundesanstalt.
- Rosenberg, C. L. (2004). Shear zones and magma ascent: A model based on a review of the Tertiary magmatism in the Alps. *Tectonics*, 23(3), TC3002. https://doi.org/10.1029/2003TC001526
- Rosenberg, C. L., & Berger, A. (2009). On the causes and modes of exhumation and lateral growth of the Alps. *Tectonics*, 28(6), TC6001. https://doi.org/10.1029/2008TC002442
- doi.org/10.1029/2008TC002442

  Rosenberg, C. L., Berger, A., Bellahsen, N., & Bousquet, R. (2015). Relating orogen width to shortening, erosion, and exhumation during Alpine
- collision. *Tectonics*, 34(6), 1306–1328. https://doi.org/10.1002/2014tc003736
  Rosenberg, C. L., Brun, J.-P., Cagnard, F., & Gapais, D. (2007). Oblique indentation in the eastern Alps: Insights from laboratory experiments.
- Tectonics, 26(2), TC2003. https://doi.org/10.1029/2006tc001960
- Rosenberg, C. L., Brun, J.-P., & Gapais, D. (2004). An indentation model of the eastern Alps and the origin of the Tauern window. *Geology*, 32(11), 997–1000. https://doi.org/10.1130/g20793.1
- Rosenberg, C. L., & Garcia, S. (2011). Estimating displacement along the Brenner fault and orogen-parallel extension in the eastern Alps [Cross-section]. *International Journal of Earth Sciences*, 100(5), 1129–1145. https://doi.org/10.1007/s00531-011-0645-3
- Rosenberg, C. L., & Garcia, S. (2012). Reply to the comment of Fügenschuh et al. on the paper 'Estimating displacement along the Brenner Fault and orogen-parallel extension in the Eastern Alps' by Rosenberg and Garcia, Int J Earth Sci (Geol Rundsch) (2011) 100: 1129–1145. International Journal of Earth Sciences, 101(5), 1457–1464. https://doi.org/10.1007/s00531-011-0726-3
- Rosenberg, C. L., & Schneider, S. (2008). The western termination of the SEMP Fault (eastern Alps) and its bearing on the exhumation of the Tauern Window. *Geological Society, London, Special Publications*, 298(1), 197–218. https://doi.org/10.1144/SP298.10
- Rosenberg, C. L., Schneider, S., Scharf, A., Bertrand, A., Hammerschmidt, K., Rabaute, A., & Brun, J.-P. (2018). Relating collisional kinematics to exhumation processes in the Eastern Alps. Earth-Science Reviews, 176, 311–344. https://doi.org/10.1016/j.earscirev.2017.10.013
- Scharf, A., Handy, M. R., Favaro, S., Schmid, S. M., & Bertrand, A. (2013). Modes of orogen-parallel stretching and extensional exhumation in response to microplate indentation and roll-back subduction (Tauern Window, Eastern Alps). *International Journal of Earth Sciences*, 102(6), 1627–1654. https://doi.org/10.1007/s00531-013-0894-4
- Schmid, S. M., Aebli, H. R., Heller, F., & Zingg, A. (1989). The role of the Periadriatic Line in the tectonic evolution of the Alps. Geological Society, London, Special Publications, 45(1), 153–171. https://doi.org/10.1144/GSL.SP.1989.045.01.08
- Schmid, S. M., Fügenschuh, B., Kissling, E., & Schuster, R. (2004). Tectonic map and overall architecture of the Alpine orogen. *Eclogae Geologicae Helvetiae*, 97(1), 93–117. https://doi.org/10.1007/s00015-004-1113-x
- Schmid, S. M., & Kissling, E. (2000). The arc of the western Alps in the light of geophysical data on deep crustal structure. *Tectonics*, 19(1), 62–85. https://doi.org/10.1029/1999tc900057
- Schmid, S. M., Pfiffner, O. A., Froitzheim, N., Schönborn, G., & Kissling, E. (1996). Geophysical-geological transect and tectonic evolution of the Swiss-Italian Alps. *Tectonics*, *15*(5), 1036–1064. https://doi.org/10.1029/96TC00433
- Schmid, S. M., Scharf, A., Handy, M. R., & Rosenberg, C. L. (2013). The Tauern window (eastern Alps, Austria): A new tectonic map, with cross-sections and a tectonometamorphic synthesis [Cross-section, map]. Swiss Journal of Geosciences, 106(1), 1–32. https://doi.org/10.1007/s00015-013-0123-y
- Schmidegg, O. (1954). Achsen-und Flächengefüge beiderseits des Silltalbruches zwischen Innsbruck und Matrei. Tschermaks mineralogische und petrographische Mitteilungen, 4(1–4), 125–137. https://doi.org/10.1007/bf01140383
- Schneider, S. (2015). Exhumation mechanisms of middle and lower crust in the western Tauern Window, Eastern Alps (Doctoral dissertation). Freie Universität Berlin. Retrieved from https://refubium.fu-berlin.de/handle/fub188/8236
- Schneider, S., Hammerschmidt, K., & Rosenberg, C. L. (2013). Dating the longevity of ductile shear zones: Insight from <sup>40</sup>Ar/J<sup>39</sup>Ar in situ analyses. *Earth and Planetary Science Letters*, 369, 43–58. https://doi.org/10.1016/j.epsl.2013.03.002
- Schönborn, G. (1992). Alpine tectonics and kinematic models of the central southern Alps. Mem Sei Geol, 44, 229-393.
- Schönborn, G. (1999). Balancing cross sections with kinematic constraints: The Dolomites (northern Italy). *Tectonics*, 18(3), 527–545. https://doi.org/10.1029/1998TC900018
- Selverstone, J. (1988). Evidence for east-west crustal extension in the Eastern Alps: Implications for the unroofing history of the Tauern Window. Tectonics, 7(1), 87–105. https://doi.org/10.1029/tc007i001p00087

RUDMANN ET AL. 21 of 22

2025, 7, Downloadec

- Sieberer, A. K., Willingshofer, E., Klotz, T., Ortner, H., & Pomella, H. (2023). Inversion of extensional basins parallel and oblique to their boundaries: Inferences from analogue models and field observations from the Dolomites Indenter, European eastern Southern Alps. *Solid Earth*, 14(7), 647–681. https://doi.org/10.5194/se-14-647-2023
- Speckbacher, R., Behrmann, J. H., Nagel, T., Stipp, M., & Devey, C. W. (2011). Splitting a continent: Insights from submarine high resolution mapping of the Moresby Seamount Detachment, offshore Papua New Guinea. *Geology*, 39(7), 651–654. https://doi.org/10.1130/G31931.1
- Staub, R. (1924). Der Bau der Alpen Versuch einer Synthese. In Beiträge zur geologischen Karte der Schweiz (52, N. F. 82). Francke.
- Stipp, M., Fügenschuh, B., Gromet, L. P., Stünitz, H., & Schmid, S. M. (2004). Contemporaneous plutonism and strike-slip faulting: A case study from the Tonale fault zone north of the Adamello pluton (Italian Alps). *Tectonics*, 23(3). https://doi.org/10.1029/2003TC001515
- Stipp, M., Stünitz, H., Heilbronner, R., & Schmid, S. M. (2002a). Dynamic recrystallization of quartz: Correlation between natural and experimental conditions. Geological Society, London, Special Publications, 200(1), 171–190. https://doi.org/10.1144/GSL.SP.2001.200.01.11
- Stipp, M., Stünitz, H., Heilbronner, R., & Schmid, S. M. (2002b). The eastern Tonale fault zone: A "natural laboratory" for crystal plastic deformation of quartz over a temperature range from 250°C to 700°C. *Journal of Structural Geology*, 24, 1861–1884.
- Stöckhert, B., Brix, M. R., Kleinschrodt, R., Hurford, A. J., & Wirth, R. (1999). Thermochronometry and microstructures of quartz A comparison with experimental flow laws and predictions on the temperature of the brittle plastic transition. *Journal of Structural Geology*, 21(3), 351–369. https://doi.org/10.1016/S0191-8141(98)00114-X
- Stünitz, H., & Gerald, J. F. (1993). Deformation of granitoids at low metamorphic grade. II: Granular flow in albite-rich mylonites. *Tectonophysics*, 221(3–4), 299–324. https://doi.org/10.1016/0040-1951(93)90164-F
- Tanner, D. C., Behrmann, J. H., & Dresmann, H. (2003). Three-dimensional retro-deformation of the Lechtal nappe, northern calcareous Alps. Journal of Structural Geology, 25(5), 737–748. https://doi.org/10.1016/S0191-8141(02)00057-3
- Thiele, O. (1980). Das Tauernfenster. In R. Oberhauser (Ed.), Der Geologische Aufbau Österreichs (pp. 300-314). Springer.
- Töchterle, A. (2011). Aspects of the geological evolution of the northwestern Tauern Window (Doctoral dissertation). University of Innsbruck,
- Töchterle, A., Brandner, R., & Reiter, F. (2007). Geologisches Tiefenprofil 1:100.000 entlang der Trasse des geplanten Brenner-Basistunnels [Cross-section, Map]. Posterbeilage im Tagungsband "BBT 2007. In Internationales Symposium Brenner Basistunnel und Zulaufstrecken, I. März 2007. Innshruck
- Töchterle, A., Brandner, R., & Reiter, F. (2011). Strain partitioning on major fault zones in the northwestern Tauern Window—Insights from the investigations of the Brenner base tunnel. *Austrian Journal of Earth Sciences*, 104(1), 15–35.
- TRANSALP Working Group, Gebrande, H., Lüschen, E., Bopp, M., Bleibinhaus, F., Lammerer, B., et al. (2002). First deep seismic reflection images of the Eastern Alps reveal giant crustal wedges and transcrustal ramps. *Geophysical Research Letters*, 29(10), 1452. https://doi.org/10.1029/2002GL014911
- van Daalen, M., Heilbronner, R., & Kunze, K. (1999). Orientation analysis of localized shear deformation in quartz fibres at the brittle–ductile transition. *Tectonophysics*, 303(1-4), 83–107. https://doi.org/10.1016/S0040-1951(98)00264-9
- Verwater, V. F., Le Breton, E., Handy, M. R., Picotti, V., Jozi Najafabadi, A., & Haberland, C. (2021). Neogene kinematics of the Giudicarie Belt and eastern Southern Alpine orogenic front (northern Italy). Solid Earth, 12(6), 1309–1334. https://doi.org/10.5194/se-12-1309-2021
- Veselá, P., & Lammerer, B. (2008). The Pfitsch-Mörchner basin, an example of the post-Variscan sedimentary evolution in the Tauern window (eastern Alps). Swiss Journal of Geosciences, 101, 73–88. https://doi.org/10.1007/s00015-008-1293-x
- Veselá, P., Lammerer, B., Wetzel, A., Söllner, F., & Gerdes, A. (2008). Post-variscan to early Alpine sedimentary basins in the Tauern window (eastern Alps). Geological Society, London, Special Publications, 298(1), 83–100. https://doi.org/10.1144/SP298.5
- Veselá, P., Oriolo, S., Basei, M. A. S., Lammerer, B., & Siegesmund, S. (2022). The detrital zircon record of Variscan to post-Variscan tectonosedimentary and magmatic processes in the Tauern Window (Eastern Alps). *International Journal of Earth Sciences*, 111(4), 1273–1287. https://doi.org/10.1007/s00531-022-02179-0
- Veselá, P., Söllner, F., Finger, F., & Gerdes, A. (2011). Magmato-sedimentary Carboniferous to Jurassic evolution of the western Tauern window, Eastern Alps (constraints from U-Pb zircon dating and geochemistry). *International Journal of Earth Sciences*, 100(5), 993–1027. https://doi. org/10.1007/s00531-010-0596-0
- Villani, F., Antonioli, A., Pastori, M., Baccheschi, P., & Ciaccio, M. G. (2024). Stress patterns and crustal anisotropy in the Eastern Alps: Insights from seismological and geological observations. *Tectonics*, 43(3), e2023TC008033. https://doi.org/10.1029/2023TC008033
- von Blanckenburg, F., & Davies, J. H. (1995). Slab breakoff: A model for syncollisional magmatism and tectonics in the Alps. *Tectonics*, 14(1), 120–131. https://doi.org/10.1029/94TC02051
- von Blanckenburg, F., Villa, I. M., Baur, H., Morteani, G., & Steiger, R. H. (1989). Time calibration of a PT-path from the western Tauern window, eastern Alps: The problem of closure temperatures [Dataset]. *Contributions to Mineralogy and Petrology*, 101, 1–11. https://doi.org/10.1007/bf00387196
- von Raumer, J. F. (1998). The Paleozoic evolution in the Alps: From Gondwana to Pangea. Geologische Rundschau, 87(3), 407–435. https://doi.org/10.1007/s005310050219
- White, S. (2001). Textural and microstructural evidence for semi-brittle flow in natural fault rocks with varied mica contents. *International Journal of Earth Sciences*, 90(1), 14–27. https://doi.org/10.1007/s005310000166
- Wilkerson, M. S., & Dicken, C. L. (2001). Quick-look techniques for evaluating two-dimensional cross sections in detached contractional settings. AAPG Bulletin, 85(10), 1759–1770. https://doi.org/10.1306/8626d063-173b-11d7-8645000102c1865d
- Wintsch, R. P., Christoffersen, R., & Kronenberg, A. K. (1995). Fluid-rock reaction weakening of fault zones. *Journal of Geophysical Research*, 100(B7), 13021–13032. https://doi.org/10.1029/94JB02622
- Wolff, R., Hetzel, R., Dunkl, I., Anczkiewicz, A. A., & Pomella, H. (2020). Fast cooling of normal-fault footwalls: Rapid fault slip or thermal relaxation? *Geology*, 48(4), 333–337. https://doi.org/10.1130/G46940.1
- Woodward, N. B., Boyer, S. E., & Suppe, J. (1989). Balanced geological cross-sections. Short course in geology, 6, 132.

RUDMANN ET AL. 22 of 22